

Joint Subarray Selection, User Scheduling, and Pilot Assignment for XL-MIMO

Gabriel Avanzi Ubiali*, José Carlos Marinello Filho†, Taufik Abrão*

* Department of Electrical Engineering, State University of Londrina (UEL), Londrina, Brazil

†Department of Electrical Engineering, Federal Technological University of Paraná (UTFPR), Cornélio Procópio, Brazil

E-mail: gabriel.ubiali@uel.br, jcmarinello@utfpr.edu.br, taufik@uel.br

Abstract

Extra-large scale MIMO (XL-MIMO) is a key technology for meeting sixth-generation (6G) requirements for high-rate connectivity and uniform quality of service (QoS); however, its deployment is challenged by the prohibitive complexity of resource management based on instantaneous channel state information (CSI). To address this intractability, this work derives novel closed-form deterministic signal-to-interference-plus-noise ratio (SINR) expressions for both centralized and distributed uplink operations. Valid for Rician fading channels with minimum mean square error (MMSE) receive combining and MMSE channel estimation, these expressions depend exclusively on long-term channel statistics, providing a tractable alternative to computationally expensive instantaneous CSI-driven optimization. Building on these results, we develop statistical-CSI-based algorithms for joint subarray selection, users scheduling, and pilot assignment, leveraging the derived SINR approximations to maximize the minimum spectral efficiency (SE) among scheduled users while preserving computational tractability. The proposed framework exploits the spatial sparsity of user equipment (UE) visibility regions (VRs) to enable more aggressive pilot reuse than is possible in conventional massive MIMO. Numerical results validate the high accuracy of the derived SINR approximations and demonstrate that the proposed algorithms significantly enhance fairness and throughput in crowded scenarios.

Index Terms

XL-MIMO, deterministic SINR, large-scale fading (LSF) subarray selection, user scheduling, pilot assignment, fairness, spectral efficiency.

I. INTRODUCTION

The evolution toward 6G networks demands unprecedented SE and link reliability [1]–[4]. XL-MIMO, characterized by antenna deployments with hundreds or thousands of elements, have emerged as a key enabling technology to meet these requirements [5]–[8]. Unlike co-located massive MIMO, XL-MIMO features antenna arrays distributed over large areas (typically organized into discrete subarrays), introducing near-field effects and spatial non-stationarity that fundamentally alter system design principles [1], [9], [10].

In XL-MIMO deployments, each UE is typically close to only a few subarrays. Consequently, serving each UE with all antennas is neither necessary nor scalable. Intelligent subarray selection ensures UEs are served only by subarrays contributing significantly to their signal, preserving service quality while reducing computational complexity [5], [11], [12]. Furthermore, in dense scenarios where UEs outnumber spatial degrees of freedom, user scheduling is essential to manage interference and satisfy QoS constraints [13], [14].

A fully centralized uplink architecture, where a central processing unit (CPU) performs joint detection, achieves the highest SE by enabling global interference suppression [15]. However, its deployment is often limited by fronthaul constraints. A more scalable alternative is distributed processing, where channel estimation and data detection are performed locally at the subarrays. This enhances implementation flexibility and scalability, as new subarrays can be integrated without upgrading the CPU [5, Sec. 5.2].

Coherent processing relies on accurate CSI. While ideally UEs would use orthogonal pilot sequences, pilot reuse is often needed due to limited channel coherence blocks [5], [16]. Pilot sharing reduces estimation accuracy and induces statistical dependence between channel estimates. Fortunately, the spatial sparsity of VRs in XL-MIMO permits more aggressive pilot reuse than in conventional massive MIMO, where every scheduled UE is “seen” by all antennas.

We develop statistical-CSI-based algorithms for joint subarray selection, user scheduling, and pilot assignment. Our key innovation lies in the use of deterministic SINR approximations derived from channel statistics. Because these expressions depend on slowly varying statistical CSI rather than instantaneous CSI, they remain valid over multiple coherence blocks. This significantly reduces computational and signaling overhead, providing a highly efficient framework for resource allocation. Furthermore, channel hardening in XL-MIMO ensures that statistical-CSI-driven algorithm achieves SE comparable to schemes relying on instantaneous CSI.

A. Related Works

Deterministic SINR expressions have been extensively investigated in multi-user massive MIMO, XL-MIMO, and cell-free architectures. However, most existing expressions are derived under spatially uncorrelated Rayleigh fading with simple maximum-ratio (MR) processing, which performs poorly in interference-limited regimes. In realistic 6G micro-urban environments, channels are characterized by a combination of line-of-sight (LoS) and non-LoS (NLoS) components, best captured by the Rician fading model. Furthermore, while MR is analytically convenient, MMSE combining is essential for interference suppression in dense networks [15].

The literature regarding deterministic SINR can be categorized by channel models and combining schemes. Expressions for spatially uncorrelated Rician fading are available in [17]–[23], but assume MR processing or perfect CSI. Conversely, works focusing on spatially correlated Rayleigh fading, such as [24]–[26] for perfect CSI and [27]–[33] for imperfect CSI, neglect the LoS component and generally restrict analysis to MR combiners, thereby limiting their applicability in dense deployments. Regarding other combining schemes, [25] and [33] investigate zero-forcing (ZF) and regularized ZF (RZF) variants, under perfect and imperfect CSI, respectively.

More recent efforts have addressed spatially correlated Rician fading with imperfect CSI and MR processing [23], [34]–[38]. A notable exception is [38], which analyzes RZF precoding. However, the resulting expressions are not fully closed-form, requiring iterative solutions of coupled fixed-point equations.

To the best of our knowledge, no existing work provides closed-form deterministic SINR expressions that jointly account for: (i) spatially correlated Rician fading, (ii) under imperfect CSI, where channel estimates are obtained via MMSE estimation, and (iii) MMSE receive combining. This paper fills this gap, providing a robust analytical framework for both centralized and distributed operations.

B. Contributions

This paper's contributions are summarized as:

- **Novel closed-form deterministic SINR expressions:** We derive original, closed-form deterministic expressions for the uplink SINR under both centralized and distributed XL-MIMO operations. These expressions are unique in that they jointly account for spatially correlated Rician fading, MMSE receive combining, and imperfect CSI obtained through MMSE channel estimation. By depending exclusively on statistical CSI, they enable rapid performance evaluation and provide a tractable analytical foundation for optimization. Numerical results validate that these approximations closely track the true SINR.

- **Statistical-CSI-driven resource allocation:** We develop algorithms for joint subarray selection, user scheduling, and pilot assignment that leverage the derived SINR approximations to maximize the minimum SE among the scheduled UEs. By utilizing only slowly-varying channel statistics, the proposed methods drastically reduce computational complexity and signaling overhead compared to instantaneous-CSI benchmarks while maintaining near-optimal performance. Numerical results demonstrate that our statistical approach closely matches the performance of instantaneous-CSI-based strategies.

II. XL-MIMO CHANNEL AND SYSTEM MODELS

Consider a system with L subarrays, coordinated by a CPU, serving K single-antenna UEs. Each subarray utilizes a uniform planar array (UPA) with M antennas. Defining the sets of all subarrays and UEs as $\mathcal{D} = \{1, \dots, L\}$ and $\mathcal{K} = \{1, \dots, K\}$, respectively, we denote $\mathcal{U} \subseteq \mathcal{K}$ as the set of scheduled UEs.

Each UE $k \in \mathcal{U}$ is served by a subarray subset $\mathcal{D}_k \subseteq \mathcal{D}$ of cardinality $L_k = |\mathcal{D}_k|$, while subarray l serves a UE subset $\mathcal{U}_l \subseteq \mathcal{U}$ of size $U_l = |\mathcal{U}_l|$. For convenience, define the selection matrix $\mathbf{D}_k = \text{blkdiag}(\mathbf{D}_{k1}, \dots, \mathbf{D}_{kL})$, where

$$\mathbf{D}_{kl} = \begin{cases} \mathbf{I}_M & \text{if } l \in \mathcal{D}_k, \\ \mathbf{0}_M & \text{otherwise.} \end{cases} \quad (1)$$

We define three subarray selection criteria: *random*; *LSF-based*, which prioritizes signal strength by selecting subarrays with the highest large-scale fading (LSF) channel gains; and *SINR-based*, which optimizes the trade-off between signal power and interference by selecting subarrays with the highest local SINRs.

During uplink data transmission, subarray l receives the signal

$$\mathbf{y}_l^{\text{ul}} = \sum_{i \in \mathcal{U}} \mathbf{h}_{il} x_i + \mathbf{n}_l^{\text{ul}}, \quad (2)$$

where \mathbf{h}_{il} is the channel vector between UE i and subarray l , $x_i \in \mathbb{C}$ is the zero-mean symbol transmitted by UE i , with transmit power $p_i = \mathbb{E}\{|x_i|^2\}$, and $\mathbf{n}_l^{\text{ul}} \sim \mathcal{N}_{\mathbb{C}}(\mathbf{0}, \sigma_n^2 \mathbf{I}_M)$ denotes the additive white Gaussian noise (AWGN) vector.

The channel vector between UE k and subarray l comprises a deterministic LoS component, $\bar{\mathbf{h}}_{kl}$, and a stochastic NLoS component, $\check{\mathbf{h}}_{kl} \sim \mathcal{N}_{\mathbb{C}}(\mathbf{0}, \mathbf{R}_{kl})$, where $\mathbf{R}_{kl} \in \mathbb{C}^{M \times M}$ is the spatial covariance matrix. It follows the distribution $\mathbf{h}_{kl} \sim \mathcal{N}_{\mathbb{C}}(\omega_{kl} \bar{\mathbf{h}}_{kl}, \mathbf{R}_{kl})$, where $\omega_{kl} \in \{0, 1\}$ is a Bernoulli random

variable indicating the presence of a LoS path. The average channel gain between UE k and the antennas of subarray l is

$$\beta_{kl} = \frac{1}{M} \mathbb{E}\{\|\mathbf{h}_{kl}\|^2\} = \frac{1}{M} \text{tr}(\mathbf{Q}_{kl}), \quad (3)$$

where $\mathbf{Q}_{kl} = \mathbb{E}\{\mathbf{h}_{kl}\mathbf{h}_{kl}^H\} = \bar{\mathbf{h}}_{kl}\bar{\mathbf{h}}_{kl}^H + \mathbf{R}_{kl}$ is the channel correlation matrix. Similarly, the channel gain associated only to the NLoS component is $\check{\beta}_{kl} = \frac{1}{M} \text{tr}(\mathbf{R}_{kl})$. The average LSF channel gain across all L subarrays for UE k is $\beta_k = \frac{1}{L} \sum_{l=1}^L \beta_{kl}$.

In modular XL-MIMO, the large inter-subarray spacing justifies modeling the NLoS channels of different subarrays as statistically independent. Hence, $\mathbb{E}\{\check{\mathbf{h}}_{kl}\check{\mathbf{h}}_{kl}^H\} = \mathbf{R}_{kl}\delta_{ll'}$, where $\delta_{ll'}$ is the Kronecker delta. As a result, the overall channel covariance matrix for user k is taken as a block-diagonal matrix, $\mathbf{R}_k = \text{blkdiag}(\mathbf{R}_{k1}, \mathbf{R}_{k2}, \dots, \mathbf{R}_{kL})$, and the collective channel vector $\mathbf{h}_k = [\mathbf{h}_{k1}^T, \dots, \mathbf{h}_{kL}^T]^T \in \mathbb{C}^{ML}$ is distributed as $\mathbf{h}_k \sim \mathcal{N}_{\mathbb{C}}(\bar{\mathbf{h}}_k, \mathbf{R}_k)$, where $\bar{\mathbf{h}}_k = [\bar{\mathbf{h}}_{k1}^T, \dots, \bar{\mathbf{h}}_{kL}^T]^T$.

A. MMSE Channel Estimation

The CPU is assumed to have perfect knowledge of the channel statistics (mean vectors and covariance matrices), as these remain approximately constant over numerous coherence blocks.¹ Under time-division-duplexing (TDD) operation, instantaneous channels are estimated via uplink pilot signaling. Each coherence block of length τ_c consists of τ_p symbols reserved for pilots and $\tau_c - \tau_p$ symbols dedicated to data transmission. This study focuses exclusively on the uplink data transmission. The pilot assigned to UE k is denoted by t_k , and its corresponding sequence is $\phi_{t_k} \in \mathbb{C}^{\tau_p}$. The sequences form an orthogonal set:

$$\phi_{t_k}^H \phi_{t_i} = \begin{cases} \tau_p, & t_i = t_k, \\ 0, & \text{otherwise.} \end{cases} \quad (4)$$

Let $\mathcal{P}_t = \{k \in \mathcal{K} \mid t_k = t\}$ denote the set of UEs using pilot t . The MMSE estimator exploits the channel statistics to separate pilot-sharing UEs and minimize the estimation mean square error (MSE). Denote by $\hat{\mathbf{h}}_{kl}$ the MMSE estimate of \mathbf{h}_{kl} and by $\tilde{\mathbf{h}}_{kl} = \mathbf{h}_{kl} - \hat{\mathbf{h}}_{kl}$ the corresponding estimation error. They are independent and distributed as [40]:

$$\hat{\mathbf{h}}_{kl} \sim \mathcal{N}_{\mathbb{C}}\left(\bar{\mathbf{h}}_{kl}, \mathbf{R}_{kl} - \mathbf{C}_{kl}\right), \quad (5)$$

$$\tilde{\mathbf{h}}_{kl} \sim \mathcal{N}_{\mathbb{C}}(\mathbf{0}_M, \mathbf{C}_{kl}), \quad (6)$$

¹Such statistics can be acquired during connection setup [39].

where the error covariance matrix is

$$\mathbf{C}_{kl} = \mathbf{R}_{kl} - p_k \tau_p \mathbf{R}_{kl} \Psi_{tl}^{-1} \mathbf{R}_{kl}, \quad (7)$$

and $\Psi_{tl} = \sum_{i \in \mathcal{P}_t} p_i \tau_p \mathbf{R}_{il} + \sigma_n^2 \mathbf{I}_M$.

The estimation accuracy can be measured by the normalized mean square error (NMSE), evaluated in subarray l and in the entire array by, respectively [5]:

$$\gamma_{kl} = \frac{\mathbb{E}\{\|\tilde{\mathbf{h}}_{kl}\|^2\}}{\mathbb{E}\{\|\mathbf{h}_{kl}\|^2\}} = \frac{\text{tr}(\mathbf{C}_{kl})}{\text{tr}(\mathbf{Q}_{kl})}, \quad (8)$$

$$\gamma_k = \frac{\mathbb{E}\{\|\tilde{\mathbf{h}}_k\|^2\}}{\mathbb{E}\{\|\mathbf{h}_k\|^2\}} = \frac{\text{tr}(\mathbf{C}_k)}{\text{tr}(\mathbf{Q}_k)}, \quad (9)$$

where $\mathbf{C}_k = \text{blkdiag}(\mathbf{C}_{k1}, \dots, \mathbf{C}_{kL})$, $\tilde{\mathbf{h}}_k = [\tilde{\mathbf{h}}_{k1}^T, \dots, \tilde{\mathbf{h}}_{kL}^T]^T$, and $\mathbf{Q}_k = \mathbb{E}\{\mathbf{h}_k \mathbf{h}_k^H\} = \bar{\mathbf{h}}_k \bar{\mathbf{h}}_k^H + \mathbf{R}_k$.

B. Centralized Uplink Operation

In centralized operation, the CPU computes the collective receive combiner $\mathbf{v}_k = [\mathbf{v}_{k1}^T, \dots, \mathbf{v}_{kL}^T]^T$ and jointly processes the uplink signals from the selected subarrays to estimate x_k , resulting in $\hat{x}_k = \mathbf{v}_k^H \mathbf{D}_k \mathbf{y}^{\text{ul}}$, where $\mathbf{y}^{\text{ul}} = [(\mathbf{y}_1^{\text{ul}})^T, \dots, (\mathbf{y}_L^{\text{ul}})^T]^T$. The instantaneous, centralized uplink SINR for UE k is given by [5, Ch. 5]

$$\Gamma_k^{\text{cent}} = \frac{p_k |\mathbf{v}_k^H \mathbf{D}_k \hat{\mathbf{h}}_k|^2}{\mathbf{v}_k^H \mathbf{D}_k \mathbf{Z}_k \mathbf{D}_k \mathbf{v}_k}, \quad (10)$$

where $\hat{\mathbf{h}}_k = [\hat{\mathbf{h}}_{k1}^T, \dots, \hat{\mathbf{h}}_{kL}^T]^T$,

$$\mathbf{Z}_k = \mathbf{W} - p_k \mathbf{D}_k \hat{\mathbf{h}}_k \hat{\mathbf{h}}_k^H \mathbf{D}_k, \quad (11)$$

and

$$\mathbf{W} = \sum_{i \in \mathcal{U}} p_i \mathbf{D}_k (\hat{\mathbf{h}}_i \hat{\mathbf{h}}_i^H + \mathbf{C}_i) \mathbf{D}_k + \sigma_n^2 \mathbf{I}_{ML}. \quad (12)$$

This SINR is maximized by the MMSE combining vector, which is given by [5, Ch. 5]

$$\mathbf{v}_k = p_k \mathbf{W}^{-1} \mathbf{D}_k \hat{\mathbf{h}}_k, \quad (13)$$

and yields the maximum SINR value

$$\Gamma_k^{\text{cent}} = p_k \hat{\mathbf{h}}_k^H \mathbf{D}_k \mathbf{Z}_k^{-1} \mathbf{D}_k \hat{\mathbf{h}}_k. \quad (14)$$

The resulting SE is given by $\eta_k^{\text{cent}} = g(\Gamma_k^{\text{cent}})$, where

$$g(x) = \left(1 - \frac{\tau_p}{\tau_c}\right) \log_2(1 + x). \quad (15)$$

As we focus exclusively on the uplink, the SE expression assumes that each channel coherence block is divided into uplink pilot transmission and uplink data transmission, ignoring downlink slots.

C. Distributed Uplink Operation

In the distributed scheme, each serving subarray $l \in \mathcal{D}_k$ first estimates the uplink symbol of UE k using the local combining vector \mathbf{v}_{kl} as:

$$\hat{x}_{kl} = \mathbf{v}_{kl}^H \mathbf{y}_l^{\text{ul}}, \quad l \in \mathcal{D}_k. \quad (16)$$

Subsequently, the CPU forms the final estimate \hat{x}_k by aggregating these local estimates:

$$\hat{x}_k = \sum_{l \in \mathcal{D}_k} \mu_{kl} \hat{x}_{kl}. \quad (17)$$

The weights satisfy $\sum_{l \in \mathcal{D}_k} \mu_{kl} = 1$ for all $k \in \mathcal{U}$, where $\mu_{kl} > 0$ if $l \in \mathcal{D}_k$, and $\mu_{kl} = 0$ otherwise.

The instantaneous local SINR for UE k evaluated at a subarray l that serves this UE is given by [5, Ch. 5]

$$\Gamma_{kl}^{\text{dist}} = \frac{p_k \left| \mathbf{v}_{kl}^H \hat{\mathbf{h}}_{kl} \right|^2}{\sum_{\substack{i \in \mathcal{U} \\ i \neq k}} p_i \left| \mathbf{v}_{kl}^H \hat{\mathbf{h}}_{il} \right|^2 + \sum_{i \in \mathcal{U}} p_i \mathbf{v}_{kl}^H \mathbf{C}_{il} \mathbf{v}_{kl} + \sigma_n^2 \left\| \mathbf{v}_{kl} \right\|^2}. \quad (18)$$

This SINR is maximized by the local MMSE (L-MMSE) combiner, given by [5, page 149]

$$\mathbf{v}_{kl} = p_k \mathbf{W}_l^{-1} \hat{\mathbf{h}}_{kl}, \quad (19)$$

which yields the maximum value

$$\Gamma_{kl}^{\text{dist}} = p_k \hat{\mathbf{h}}_{kl}^H \mathbf{Z}_{kl}^{-1} \hat{\mathbf{h}}_{kl} = p_k \text{tr} \left(\mathbf{Z}_{kl}^{-1} \hat{\mathbf{h}}_{kl} \hat{\mathbf{h}}_{kl}^H \right), \quad (20)$$

where

$$\mathbf{W}_l = \sum_{i \in \mathcal{U}} p_i (\hat{\mathbf{h}}_{il} \hat{\mathbf{h}}_{il}^H + \mathbf{C}_{il}) + \sigma_n^2 \mathbf{I}_M \quad (21)$$

and

$$\mathbf{Z}_{kl} = \mathbf{W}_l - p_k \hat{\mathbf{h}}_{kl} \hat{\mathbf{h}}_{kl}^H. \quad (22)$$

The global SINR for UE k under distributed operation, denoted as Γ_k^{dist} , is given by (23), and the resulting SE is given by $\eta_k^{\text{dist}} = g(\Gamma_k^{\text{dist}})$.

$$\Gamma_k^{\text{dist}} = \frac{p_k \left| \sum_{l \in \mathcal{D}_k} \mu_{kl} \mathbf{v}_{kl}^H \hat{\mathbf{h}}_{kl} \right|^2}{\sum_{i \in \mathcal{U} \setminus \{k\}} p_i \left| \sum_{l \in \mathcal{D}_k} \mu_{kl} \mathbf{v}_{kl}^H \hat{\mathbf{h}}_{il} \right|^2 + \sum_{i \in \mathcal{U}} p_i \sum_{l \in \mathcal{D}_k} \mu_{kl}^2 \mathbf{v}_{kl}^H \mathbf{C}_{il} \mathbf{v}_{kl} + \sigma_n^2 \sum_{l \in \mathcal{D}_k} \mu_{kl}^2 \|\mathbf{v}_{kl}\|^2}. \quad (23)$$

Proposition 1 (Global SINR Approximation and Optimal Weights). *Assuming $M \geq U$ and L -MMSE combining, the global SINR for UE k can be approximated by:*

$$\hat{\Gamma}_k^{\text{dist}} = \left(\sum_{l \in \mathcal{D}_k} \mu_{kl}^2 (\Gamma_{kl}^{\text{dist}})^{-1} \right)^{-1}. \quad (24)$$

The weights that maximize (24) subject to $\sum_{l \in \mathcal{D}_k} \mu_{kl} = 1$ are:

$$\mu_{kl} = \begin{cases} \frac{\Gamma_{kl}^{\text{dist}}}{\sum_{l' \in \mathcal{D}_k} \Gamma_{kl'}^{\text{dist}}}, & \text{if } l \in \mathcal{D}_k, \\ 0, & \text{otherwise,} \end{cases} \quad (25)$$

yielding the maximum approximate global SINR

$$\hat{\Gamma}_k^{\text{dist}} = \sum_{l \in \mathcal{D}_k} \Gamma_{kl}^{\text{dist}}. \quad (26)$$

Proof. See Appendix A. \square

We also refer to the optimal weighting in (25) as SINR-based weighting. A practical alternative is LSF-based weighting, which avoids local SINR estimation by using weights proportional to the LSF gains:

$$\mu_{kl} = \begin{cases} \frac{\beta_{kl}}{\sum_{l' \in \mathcal{D}_k} \beta_{kl'}}, & \text{if } l \in \mathcal{D}_k, \\ 0, & \text{otherwise.} \end{cases} \quad (27)$$

While (27) is suboptimal as it neglects interference and channel estimation errors, it generally outperforms the equal weighting strategy, defined as:

$$\mu_{kl} = \begin{cases} 1/L_k, & \text{if } l \in \mathcal{D}_k, \\ 0, & \text{otherwise.} \end{cases} \quad (28)$$

The approximate SE can be expressed via the global mapping $\hat{\eta}_k^{\text{dist}} = g(\hat{\Gamma}_k^{\text{dist}})$ or, equivalently, via

the component-wise mapping $\hat{\eta}_k^{\text{dist}} = \hat{g}(\{\Gamma_{kl}^{\text{dist}}\}_{l \in \mathcal{D}_k})$, defined as:

$$\hat{g}(\{\Gamma_{kl}\}_{l \in \mathcal{D}_k}) = \left(1 - \frac{\tau_p}{\tau_c}\right) \log_2 \left(1 + \frac{1}{\sum_{l \in \mathcal{D}_k} \mu_{kl}^2 \Gamma_{kl}^{-1}}\right). \quad (29)$$

D. Performance Comparison

This subsection evaluates the uplink performance of centralized and distributed XL-MIMO architectures as a function of the number of serving subarrays, for different subarray selection and weighting strategies.

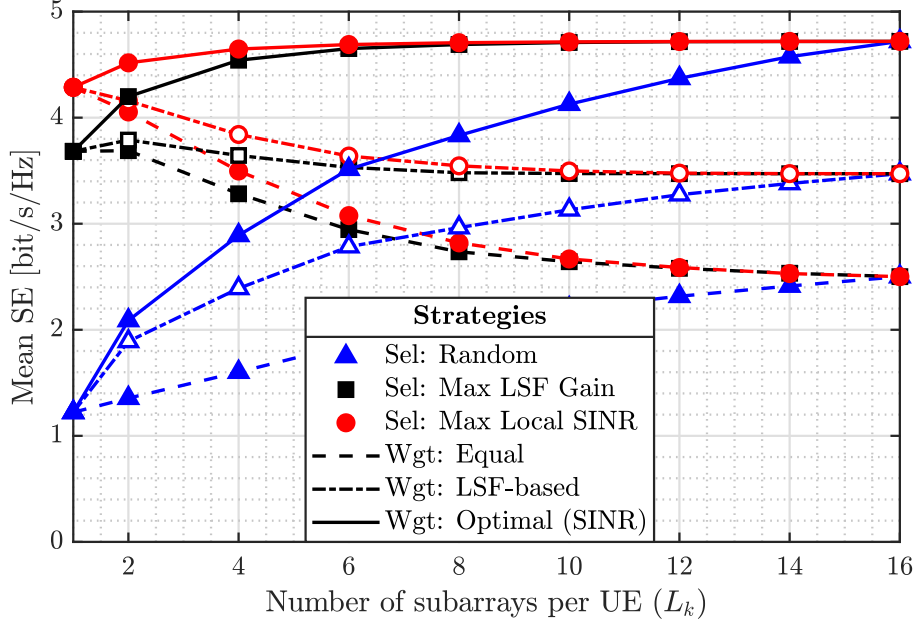
The base station (BS) comprises $L = 16$ linearly arranged subarrays, each equipped with a 4×4 UPA ($M = 16$), serving $U = 16$ UEs in a 100×50 m coverage area. The coherence block length is $\tau_c = 16$ and $\tau_p = 8$ orthogonal pilots are randomly assigned to the UEs, which implies pilot contamination since $U > \tau_p$. Table I summarizes the remaining parameter values adopted in this validation.

Table I
SIMULATION PARAMETERS

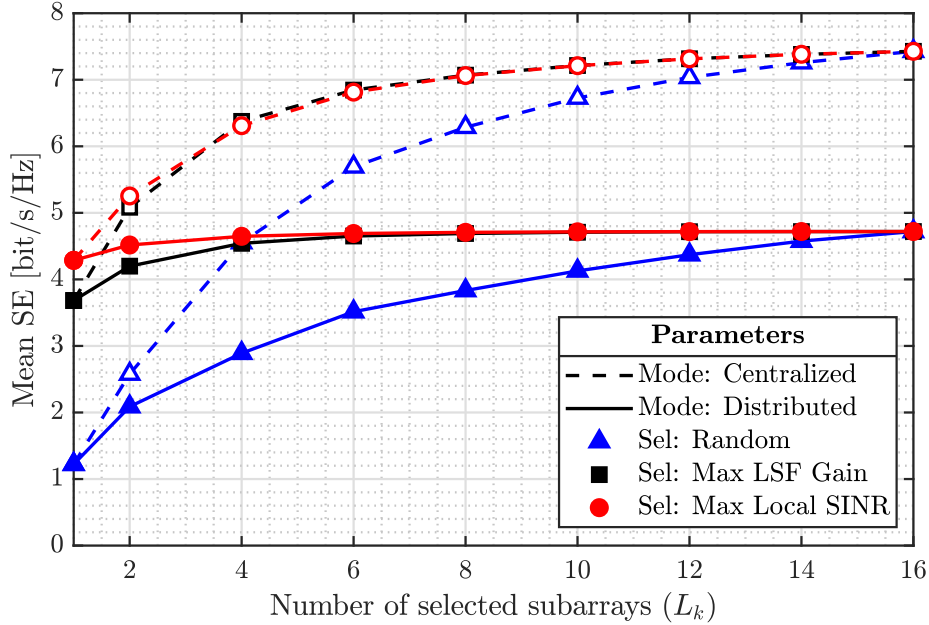
Parameter	Value
Number of subarrays (L)	16
UE transmit power (p_k)	20 dBm
Noise power (σ_n^2)	-96 dBm
Channel coherence block length (τ_c)	16
Carrier frequency	6 GHz
Antenna spacing (half-wavelength)	2.5 cm
Subarray spacing	6.0 m
Array height	3 m
UE height	1.5 m

Figure 1a illustrates the impact of subarray selection and weighting on the mean SE in distributed operation. Two distinct convergence regimes are observed at the boundaries of the L_k range. At $L_k = 1$, performance is dictated solely by the *selection* strategy, clustering the curves into three groups; weighting is irrelevant here, as the final signal estimate coincides with the local estimate from the selected subarray. Conversely, at $L_k = L = 16$, the selection strategy is irrelevant, and the curves cluster into three groups determined exclusively by the *weighting* scheme.

For small numbers of selected subarrays (e.g., $L_k = 2$), intelligent selection (LSF- and SINR-based) significantly outperforms random selection. The SINR-based scheme yields the highest performance, confirming that interference awareness is especially critical when L_k is low. As L_k increases, the LSF-based selection converges to the SINR-based scheme in performance.



(a) Distributed operation: comparing subarray selection and weighting strategies.



(b) Architecture comparison: centralized vs. distributed with optimal weighting, varying subarray selection strategy.

Figure 1. Mean SE versus number of selected subarrays L_k .

The optimal (SINR-based) weighting provides a clear upper bound, increasing monotonically with L_k up to about 4.7 bit/s/Hz. In contrast, *equal* weighting degrades performance for intelligent selection schemes as L_k grows, since it does not attenuate the contribution of the subarrays with weak channels or strong interference. Consequently, increasing L_k in distributed operation is only

beneficial if optimal weights are applied. The LSF-based weighting offers an intermediate solution, alleviating performance loss but still falling short of the optimum as it fails to penalize interference.

Figure 1b compares the distributed architecture (with optimal weighting) against the fully centralized implementation. As expected, centralized processing consistently outperforms the distributed approach due to its ability to jointly suppress inter-user interference. The *SINR-based* selection yields the highest performance for both architectures. The *LSF-based* scheme closely follows the SINR-based trend, reinforcing that LSF is a robust selection metric.

The results highlight the trade-off between complexity and SE. While centralized processing yields superior SE, the distributed architecture offers a viable low-complexity alternative. To maximize its efficacy, two design choices are critical: *a*) LSF-based subarray selection is recommended for achieving near-optimal performance without requiring local SINR estimation; and *b*) optimal weighting is mandatory to prevent performance degradation when scaling L_k .

Finally, results demonstrated that selecting only a small subset of subarrays to serve each UE is sufficient to achieve high mean SE while significantly reducing computational complexity and fronthaul load compared to utilizing the full antenna array ($L_k = L$).

III. UPLINK SINR APPROXIMATIONS

This section derives deterministic asymptotic and ergodic SINR approximations for centralized and distributed uplink operation. The asymptotic expressions describe the deterministic convergence of the instantaneous SINR as the number of antennas grows large. Conversely, the ergodic expressions approximate the average SINR and are particularly accurate in crowded scenarios with high user loads.

Theorem 1 (Ergodic SINR). *The ergodic global uplink SINR for centralized operation with MMSE combiner and the ergodic local uplink SINR for distributed operation with L-MMSE combiner are:*

$$\Gamma_k^{\text{cent,erg}} \approx p_k \text{tr} \left[\mathbf{D}_k \bar{\mathbf{Z}}_k^{-1} \mathbf{D}_k (\mathbf{Q}_k - \mathbf{C}_k) \mathbf{D}_k \right], \quad (30a)$$

$$\Gamma_{kl}^{\text{dist,erg}} \approx p_k \text{tr} \left[\bar{\mathbf{Z}}_{kl}^{-1} (\mathbf{Q}_{kl} - \mathbf{C}_{kl}) \right], \quad (30b)$$

where

$$\bar{\mathbf{Z}}_k = \mathbf{D}_k \left(\sum_{i \in \mathcal{U} \setminus \{k\}} p_i \mathbf{Q}_i + p_k \mathbf{C}_k \right) \mathbf{D}_k + \sigma_n^2 \mathbf{I}_{ML}, \quad (31a)$$

$$\bar{\mathbf{Z}}_{kl} = \sum_{i \in \mathcal{U} \setminus \{k\}} p_i \mathbf{Q}_{il} + p_k \mathbf{C}_{kl} + \sigma_n^2 \mathbf{I}_M. \quad (31b)$$

These approximations hold if the selected subarrays yield strong LoS components or under high user load conditions (i.e., $U \gg ML_k$ for centralized or $U \gg M$ for distributed operation).

Proof. See Appendix B. \square

Corollary 1. *The computational complexity (in real multiplications) to evaluate (30a) and (30b) across the L_k serving subarrays is, respectively:*

$$\mathcal{C}_k^{\text{cent,erg}} = 3M^3L_k^3 + \frac{1}{2}M^2L_k^2 - \frac{3}{2}ML_k, \quad (32\text{a})$$

$$\mathcal{C}_k^{\text{dist,erg}} = 3M^3L_k + \frac{1}{2}M^2L_k - \frac{3}{2}ML_k. \quad (32\text{b})$$

Proof. See Appendix C. \square

Theorem 2 (Asymptotic SINR). *Assume MMSE channel estimation and user loads satisfying $U \leq ML_k$ for centralized or $U \leq M$ for distributed operation. Furthermore, assume MMSE (centralized) or L-MMSE (distributed) combining is used, and that a) there is no pilot reuse or b) the channel estimates are relatively accurate and the NLoS channel component is spatially uncorrelated. As the number of antennas grows large ($ML_k \rightarrow \infty$ for centralized or $M \rightarrow \infty$ for distributed operation), the instantaneous SINR converges deterministically to the asymptotic limits given by:*

$$\Gamma_k^{\text{cent,asy}} = \frac{\text{tr}(\mathbf{D}_k \mathbf{X}_k \mathbf{D}_k) - \sum_{i \in \mathcal{U} \setminus \{k\}} \frac{\text{tr}(\mathbf{D}_k \mathbf{X}_i \mathbf{D}_k)}{\text{tr}(\mathbf{D}_k \mathbf{X}_i \mathbf{D}_k)}}{\sum_{i \in \mathcal{U}} \frac{p_i}{ML_k p_k} \text{tr}(\mathbf{D}_k \mathbf{C}_i \mathbf{D}_k) + \sigma_n^2}, \quad (33\text{a})$$

$$\Gamma_{kl}^{\text{dist,asy}} = \frac{\text{tr}(\mathbf{X}_{kl}) - \sum_{i \in \mathcal{U} \setminus \{k\}} \frac{\text{tr}(\mathbf{X}_{kl} \mathbf{X}_{il})}{\text{tr}(\mathbf{X}_{il})}}{\sum_{i \in \mathcal{U}} \frac{p_i}{M p_k} \text{tr}(\mathbf{C}_{il}) + \sigma_n^2}, \quad (33\text{b})$$

where $\mathbf{X}_k = \mathbf{Q}_k - \mathbf{C}_k$ and $\mathbf{X}_{kl} = \mathbf{Q}_{kl} - \mathbf{C}_{kl}$.

Proof. See Appendix D. \square

Corollary 2. *The computational complexity (in real multiplications) to evaluate (33a) and (33b) across the L_k serving subarrays is, respectively:*

$$\mathcal{C}_k^{\text{cent,asy}} = 3(U-1)M^2L_k^2, \quad (34\text{a})$$

$$\mathcal{C}_k^{\text{dist,asy}} = 3(U-1)M^2L_k. \quad (34\text{b})$$

Proof. Complexity is dominated by evaluating trace terms $\text{tr}(\mathbf{AB})$ for the $U-1$ interfering UEs

$(i \neq k)$. Computing the trace of a product of two square matrices of size N requires calculating only the diagonal elements of the product, costing N^2 complex multiplications. For distributed operation (33b), this involves $M \times M$ matrices ($N = M$) for each of the L_k subarrays. For centralized operation (33a), the matrices have effective size $ML_k \times ML_k$ ($N = ML_k$). Assuming three real multiplications per complex multiplication [41, p. 378], we arrive at (34a) and (34b). \square

The approximate achievable SE is obtained via the mapping $g(\cdot)$ in (15). For centralized operation, we evaluate $\eta_k^{\text{cent,asy}} = g(\Gamma_k^{\text{cent,asy}})$ and $\eta_k^{\text{cent,erg}} = g(\Gamma_k^{\text{cent,erg}})$. For distributed operation, it is reconstructed from the local SINR approximations as $\hat{\eta}_k^{\text{dist,asy}} = \hat{g}(\{\Gamma_{kl}^{\text{dist,asy}}\}_{l \in \mathcal{D}_k})$ and $\hat{\eta}_k^{\text{dist,erg}} = \hat{g}(\{\Gamma_{kl}^{\text{dist,erg}}\}_{l \in \mathcal{D}_k})$.

A. Approximation Accuracy

This section validates the derived SINR approximations. Simulations assume $L = 16$ and $L_k = 4$, employing LSF-based subarray selection and optimal weighting.² We enforce pilot contamination by setting $\tau_p = U/2$ with random assignment, while $\tau_c = U$. Remaining parameters are listed in Table I.

We assess the accuracy of the derived approximations using the mean normalized absolute error (MNAE) metric. For a generic variable x and its estimate \hat{x} , the MNAE is defined as:³

$$\nu(x, \hat{x}) = \mathbb{E} \left\{ \frac{|\hat{x} - x|}{x} \right\}. \quad (35)$$

To validate the global SINR approximation for distributed operation derived in Proposition 1, we evaluate the error between the true distributed SE and its estimate based on local SINRs:

$$\tilde{\eta}_k^{\text{dist}} = \nu(\eta_k^{\text{dist}}, \hat{\eta}_k^{\text{dist}}). \quad (36)$$

Since the asymptotic expressions target the *instantaneous* performance, their accuracy is measured relative to the true instantaneous SE:

$$\tilde{\eta}_k^{\text{op,asy}} = \nu(\eta_k^{\text{op}}, \hat{\eta}_k^{\text{op,asy}}), \quad \text{for op} \in \{\text{cent, dist}\}. \quad (37)$$

Conversely, the ergodic expressions target the *average* performance. Thus, we compare them against the true mean SE:

$$\tilde{\eta}_k^{\text{op,erg}} = \nu(\mathbb{E}\{\eta_k^{\text{op}}\}, \hat{\eta}_k^{\text{op,erg}}), \quad \text{for op} \in \{\text{cent, dist}\}. \quad (38)$$

²The choice of $L_k = 4$ is justified by the performance-complexity trade-off observed in Fig. 1b.

³Throughout this work, $\mathbb{E}\{\cdot\}$ denotes the expectation over small-scale fading (SSF) realizations.

We first assess the accuracy of the global SINR approximation for distributed operation in (24) using Fig. 2, which plots the MNAE $\tilde{\eta}_k^{\text{dist}}$ versus M .⁴ The approximation error decreases steadily with M and increases with U , since a larger M/U ratio provides stronger interference suppression, satisfying the derivation's assumption of negligible coherent interference. On the other hand, selecting fewer subarrays (e.g., $L_k = 2$), yields lower MNAE than larger subsets (e.g., $L_k = 8$), as the LSF-based strategy can restrict selection to the strongest subarrays where $\mathbf{v}_{kl}^H \hat{\mathbf{h}}_{kl} \approx 1$.⁵ These factors render the approximation robust even in the overloaded regime ($M < U$).

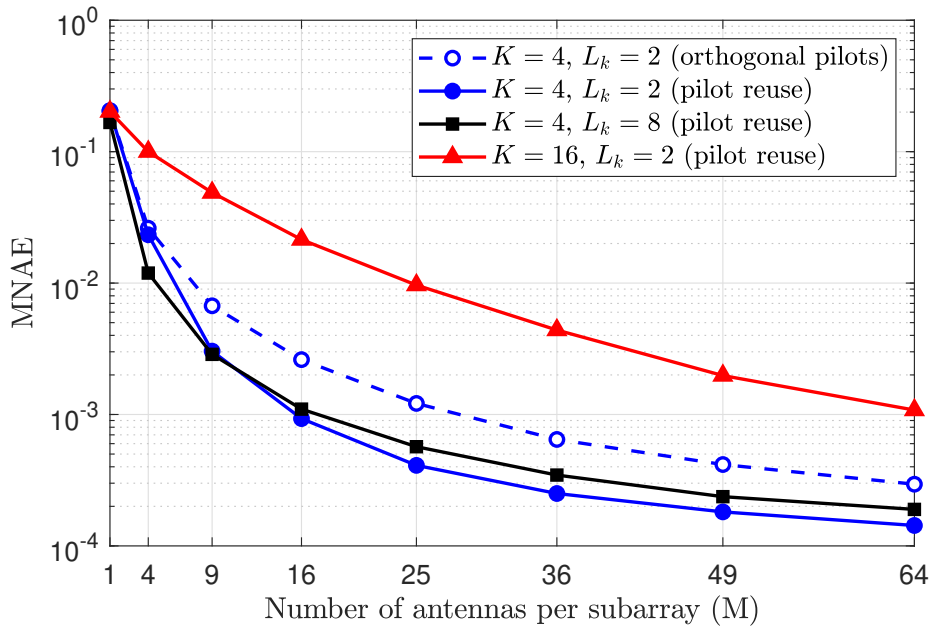


Figure 2. MNAE of the global SE approximation for distributed operation versus subarray antennas.

Figure 3 evaluates the ergodic and asymptotic approximations as a function of U , with fixed $M = 16$ and $L_k = 4$. The subfigures depict the MNAE for distributed (Fig. 3a) and centralized (Fig. 3b) operations, assessing the impact of spatial correlation and pilot contamination. To this end, we compare spatially correlated vs. uncorrelated fading, and contrast orthogonal pilot assignment ($\tau_p = U$) with pilot reuse ($\tau_p = U/2$, with random assignment).

The MNAE of the asymptotic expression increases with U . As the system load grows, the variance of the aggregate interference becomes more significant, causing the instantaneous realizations to deviate further from the deterministic limit. This divergence is more pronounced in compared to

⁴We actually plot the accuracy averaged across both scheduled UEs and channel realizations.

⁵See Appendix A for more details on the validity conditions for the approximation.

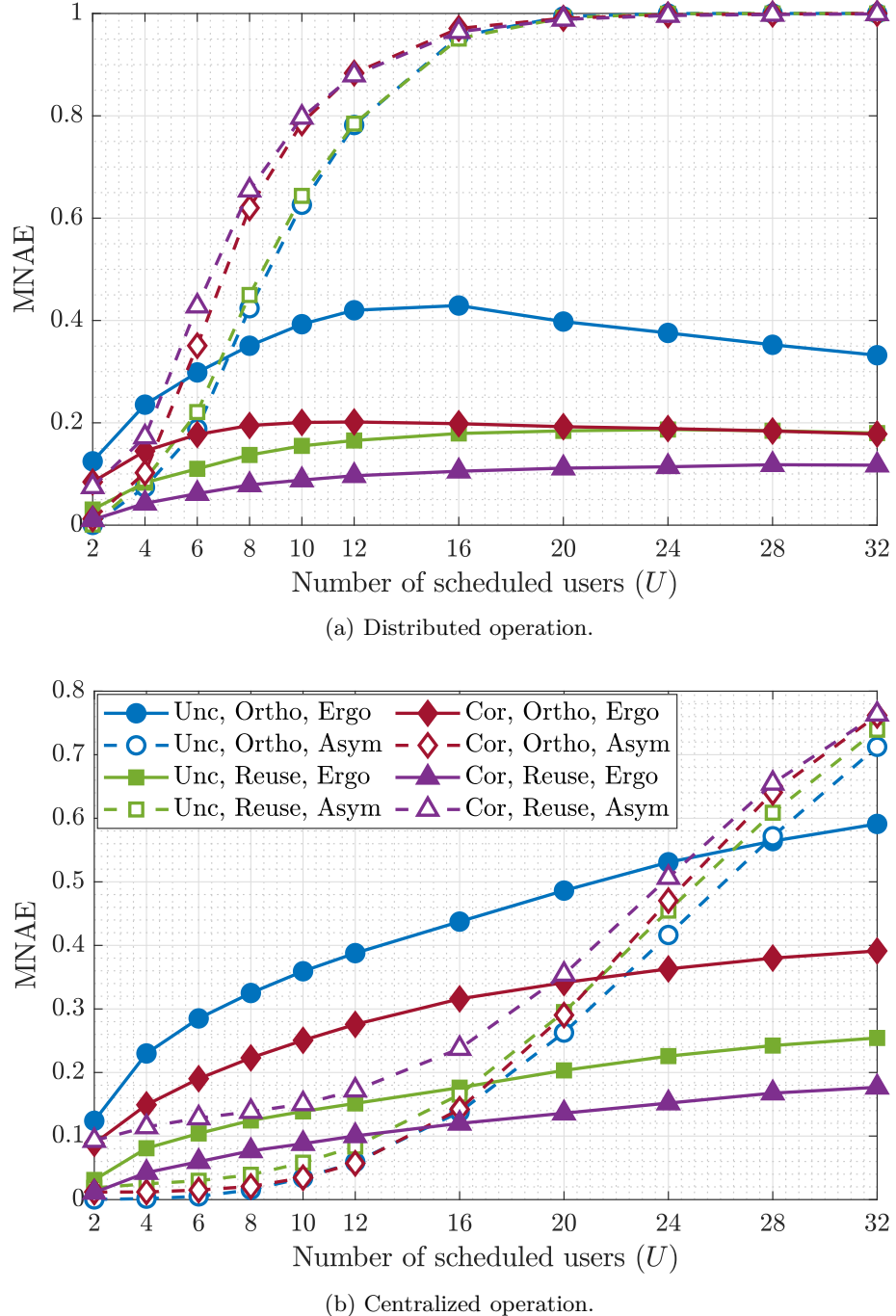


Figure 3. MNAE of the deterministic SE approximations vs. number of UEs, contrasting ergodic and asymptotic approximations under varying spatial correlation and pilot reuse scenarios.

the centralized case. The latter benefits from a higher diversity order (ML_k antennas involved in combining), which accelerates convergence to the deterministic mean.

According to Fig 3, spatial correlation and pilot reuse degrade the accuracy of the asymptotic approximations by violating the tractability assumptions underlying (33a) and (33b), which rely

on uncorrelated NLoS components and small channel estimation errors. Furthermore, correlation reduces spatial diversity, which hinders channel hardening and thereby delays the SINR convergence to the deterministic regime, while pilot contamination scales with U . These factors introduce direct modeling discrepancies, causing the instantaneous SE to diverge from the asymptotic approximation.

Counter-intuitively, spatial correlation and pilot reuse reduce the MNAE of the ergodic approximations by increasing the deterministic covariance \mathbf{C}_{kl} , which stabilizes \mathbf{Z}_{kl} around its mean, better satisfying the Neumann series condition required for these approximations. The error evolution is driven by competing effects: it initially rises with U as additional interferers increase the variance of \mathbf{Z}_{kl} , and then it peaks near the spatial degrees of freedom ($U \approx M$ for distributed operation and $U \approx ML_k$ for centralized). As we increase U beyond this peak, \mathbf{Z}_{kl} concentrates around its expected value. This explains why, for the same M , the ergodic approximation is more accurate in distributed operation than in centralized: it reaches saturation significantly earlier than the centralized.

Given the contrasting error behaviors of the ergodic and asymptotic approximations, we define a switching point, U_{switch} , to select the best approximation. The asymptotic expression is prioritized for $U \leq U_{\text{switch}}$ due to its superior accuracy and lower complexity, while the ergodic expression is adopted for $U > U_{\text{switch}}$. The optimal U_{switch} depends on channel conditions and the pilot assignment strategy, shifting toward lower values of U when correlation or pilot reuse is present. Table II summarizes the empirically determined switching thresholds derived from the intersection points of the asymptotic and ergodic error curves in Fig. 3. Note that the thresholds for centralized operation are consistently scaled by L_k compared to the distributed case. Note also that, in the most severe scenario (correlated NLoS with pilot reuse), the threshold drops to $U_{\text{switch}} \approx 0$. This indicates that the asymptotic approximation is unreliable for any practical user load under these conditions, and the ergodic approximation should be employed exclusively for all U .

Table II
SWITCHING THRESHOLD U_{switch} VALUES.

Scenario		Operation	
NLoS	Pilots	Centralized	Distributed
Uncorrelated	Orthogonal	$ML_k/2$	$M/2$
	Reuse	$ML_k/4$	$M/4$
Correlated	Orthogonal	$ML_k/4$	$M/4$
	Reuse	0	0

The validity of the asymptotic approximations relies on channel hardening, confirmed by the

monotonic MNAE decrease when increasing M in Fig. 4. Centralized operation converges significantly faster than distributed operation, achieving accuracy even at moderate M due to the larger effective array size (ML_k vs. M) involved in joint combining. Conversely, accuracy degrades with pilot reuse and higher user loads (U). The simulation setup includes spatially correlated NLoS components and $L_k = 2$.

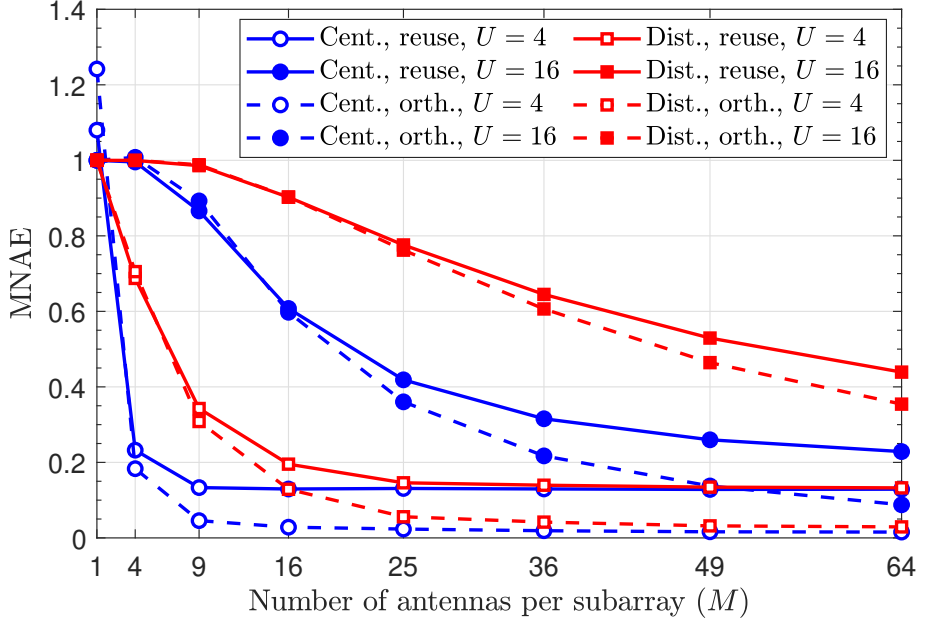


Figure 4. MNAE of the asymptotic SE approximation versus subarray antennas (M).

IV. APPLYING USER SCHEDULING, PILOT ASSIGNMENT AND SUBARRAY SELECTION IN XL-MIMO

A widely used benchmark for joint pilot assignment and subarray selection is the greedy algorithm in [5, Sec. 4.4], which follows a three-stage procedure: (i) assign τ_p orthogonal pilots to τ_p random UEs; (ii) sequentially assign pilots to the remaining UEs so as to minimize pilot contamination⁶; and (iii) perform subarray selection, where each subarray locally chooses which τ_p UEs to serve, specifically one UE per pilot (namely, the strongest UE using that pilot). While this approach ensures minimal computational complexity, it does not strictly guarantee full user scheduling, as certain UEs may remain unselected by any subarray.

⁶When assigning a candidate pilot t to a UE k , [5, Sec. 4.4] measures pilot contamination as the sum of the NLoS channel gains of the UEs already using pilot t , evaluated at UE k 's strongest subarray. Only the NLoS component is considered because the deterministic LoS component does not contribute to the channel estimation error.

This section proposes joint user scheduling and pilot assignment algorithms to enhance the minimum per-user SE. Algorithm 1 maximizes the number of scheduled UEs subject to a maximum channel estimation error threshold, γ_{th} (line 2). It iteratively schedules UEs in descending order of LSF gain (line 3). In each step, the candidate UE is assigned the pilot (either an existing or a new one) that minimizes the maximum channel estimation NMSE across the candidate user set $\tilde{\mathcal{U}}$ (lines 4-9). If the resulting maximum NMSE satisfies γ_{th} , the UE is scheduled (lines 10-12).

Algorithm 1 NMSE-Based User Scheduling & Pilot Assignment

Require:

NMSE threshold: γ_{th}
 Subarray selection sets: $\{\mathcal{D}_i\}_{i \in \mathcal{K}}$
 Channel statistics: $\{\mathbf{Q}_{kl}, \mathbf{R}_{kl}\}_{k \in \mathcal{K}, l \in \mathcal{D}}, \{\beta_k\}_{k \in \mathcal{K}}$
 Transmit powers: $\{p_k\}_{k \in \mathcal{K}}$

Ensure:

Set of scheduled users: \mathcal{U}
 Pilot indices: $\{t_k\}_{k \in \mathcal{U}}$

- 1: Initialize: $\mathcal{U} \leftarrow \emptyset, \tau_p \leftarrow 0, \gamma_{\text{max}} \leftarrow 0$
- 2: **while** $|\mathcal{U}| < K$ and $\gamma_{\text{max}} \leq \gamma_{\text{th}}$ **do**
- 3: $k \leftarrow \arg \max_{i \in \mathcal{K} \setminus \mathcal{U}} \beta_i$ and $\tilde{\mathcal{U}} \leftarrow \mathcal{U} \cup \{k\}$
- 4: **for** $t = 1$ to $\tau_p + 1$ **do**
- 5: $t_k \leftarrow t, \tau \leftarrow \max(\tau_p, t_k), \zeta \leftarrow \{1, \dots, \tau\}$
- 6: $\Psi_{\tilde{t}l} \leftarrow \sum_{i \in \tilde{\mathcal{U}}} p_i \tau \mathbf{R}_{il} + \sigma_n^2 \mathbf{I}_M, l \in \mathcal{D}, \tilde{t} \in \zeta$
- 7: $\gamma_{\text{max}}^{(t)} \leftarrow \max_{i \in \tilde{\mathcal{U}}} \frac{\sum_{l \in \mathcal{D}_i} \text{tr}(\mathbf{R}_{il} - p_i \tau \mathbf{R}_{il} \Psi_{\tilde{t}l}^{-1} \mathbf{R}_{il})}{\sum_{l \in \mathcal{D}_i} \text{tr}(\mathbf{Q}_{il})}$
- 8: **end for**
- 9: $t_k \leftarrow \arg \min_{t \in \{1, \dots, \tau_p + 1\}} \gamma_{\text{max}}^{(t)}$ and $\gamma_{\text{max}} \leftarrow \gamma_{\text{max}}^{(t_k)}$
- 10: **if** $\gamma_{\text{max}} \leq \gamma_{\text{th}}$ **then**
- 11: $\mathcal{U} \leftarrow \tilde{\mathcal{U}}$ and $\tau_p \leftarrow \max(\tau_p, t_k)$
- 12: **end if**
- 13: **end while**

Designed for centralized and distributed operation, respectively, Algorithms 2 and 3 adopt the same framework of Algorithm 1. However, rather than minimizing the maximum channel estimation NMSE, their pilot assignment criteria maximizes the minimum per-user SE, and their user scheduling strategy maximizes the number of scheduled UEs subject to a minimum per-user SE, η_{th} . More than scheduling UEs and assigning pilots, Algorithm 3 computes the optimal weights used to obtain the final signal estimates from the local estimates (lines 15 and 21).

For each candidate pilot, Algorithm 2 evaluates the SINRs of the UEs $\tilde{\mathcal{U}}$ using the ergodic approximation in (30a) when $|\tilde{\mathcal{U}}| > U_{\text{switch}}$ and the asymptotic approximation (33a) otherwise (lines 6–14), and then it estimates the minimum SE based on these SINRs (line 15). This conditional

Algorithm 2 SINR-Based Joint User Scheduling & Pilot Assignment For Centralized Operation**Require:**

Switching point: U_{switch}
 SE threshold: η_{th}
 Subarray selection matrices: $\{\mathbf{D}_k\}_{k \in \mathcal{K}}$
 Number of subarrays serving each user: $\{L_k\}_{k \in \mathcal{K}}$
 Channel statistics: $\{\mathbf{Q}_k, \mathbf{R}_k, \beta_k\}_{k \in \mathcal{K}}$
 Transmit powers: $\{p_k\}_{k \in \mathcal{K}}$

Ensure:

Set of scheduled users: \mathcal{U}
 Pilot indices: $\{t_k\}_{k \in \mathcal{U}}$

- 1: Initialize: $\mathcal{U} \leftarrow \emptyset$, $\tau_p \leftarrow 0$, $\eta_{\min} \leftarrow 2\eta_{\text{th}}$
- 2: **while** $|\mathcal{U}| < K$ and $\eta_{\min} > \eta_{\text{th}}$ **do**
- 3: $k \leftarrow \arg \max_{i \in \mathcal{K} \setminus \mathcal{U}} \beta_i$ and $\tilde{\mathcal{U}} \leftarrow \mathcal{U} \cup \{k\}$
- 4: **for** $t = 1$ to $\tau_p + 1$ **do**
- 5: $t_k \leftarrow t$, $\tau \leftarrow \max(\tau_p, t_k)$, $\zeta \leftarrow \{1, \dots, \tau\}$
- 6: $\Psi_{\tilde{t}} \leftarrow \sum_{i \in \tilde{\mathcal{U}}} p_i \tau \mathbf{R}_i + \sigma_n^2 \mathbf{I}_{ML}$, $\tilde{t} \in \zeta$
- 7: $\mathbf{C}_i \leftarrow \mathbf{R}_i - p_i \tau \mathbf{R}_i \Psi_{t_i}^{-1} \mathbf{R}_i$, $i \in \tilde{\mathcal{U}}$
- 8: **if** $|\tilde{\mathcal{U}}| > U_{\text{switch}}$ **then**: for $i \in \tilde{\mathcal{U}}$:
- 9: $\bar{\mathbf{Z}}_i \leftarrow \mathbf{D}_i \left(\sum_{\substack{i' \in \tilde{\mathcal{U}} \\ i' \neq i}} p_{i'} \mathbf{Q}_{i'} + p_i \mathbf{C}_i \right) \mathbf{D}_i + \sigma_n^2 \mathbf{I}_{ML}$
- 10: $\Gamma_i \leftarrow p_i \text{tr}[\mathbf{D}_i \bar{\mathbf{Z}}_i^{-1} \mathbf{D}_i (\mathbf{Q}_i - \mathbf{C}_i) \mathbf{D}_i]$
- 11: **else**: for $i \in \tilde{\mathcal{U}}$:
- 12: $\mathbf{S}_{ii'} \leftarrow \mathbf{D}_i (\mathbf{Q}_{i'} - \mathbf{C}_{i'}) \mathbf{D}_i$, $i' \in \tilde{\mathcal{U}}$
 $\text{tr}(\mathbf{S}_{ii}) - \sum_{i' \in \tilde{\mathcal{U}} \setminus \{i\}} \frac{\text{tr}(\mathbf{S}_{ii} \mathbf{S}_{ii'})}{\text{tr}(\mathbf{S}_{ii'})}$
- 13: $\Gamma_i \leftarrow \frac{1}{\sum_{i' \in \tilde{\mathcal{U}}} \frac{p_{i'}}{ML_i p_i} \text{tr}(\mathbf{D}_i \mathbf{C}_{i'} \mathbf{D}_i) + \sigma_n^2}$
- 14: **end if**
- 15: $\eta_{\min}^{(t)} \leftarrow \min_{i \in \tilde{\mathcal{U}}} \left(1 - \frac{\tau}{\tau_c} \right) \log_2(1 + \Gamma_i)$
- 16: **end for**
- 17: $t_k \leftarrow \arg \max_{t \in \{1, \dots, \tau_p + 1\}} \eta_{\min}^{(t)}$ and $\eta_{\min} \leftarrow \eta_{\min}^{(t_k)}$
- 18: **if** $\eta_{\min} \geq \eta_{\text{th}}$ **then**
- 19: $\mathcal{U} \leftarrow \tilde{\mathcal{U}}$ and $\tau_p \leftarrow \max(\tau_p, t_k)$
- 20: **end if**
- 21: **end while**

switching rule improves the accuracy of the SINR estimates by selecting the analytical expression that is known to be more reliable for each loading regime. Its value is chosen based on the numerical analysis in Section III-A.

Similarly, Algorithm 3 evaluates the resulting SINRs for each candidate pilot using (30b) when $|\tilde{\mathcal{U}}| > U_{\text{switch}}$ and (33b) otherwise (lines 6–14). Since optimal weighting is employed, line 16 approxi-

Algorithm 3 SINR-Based Joint User Scheduling & Pilot Assignment For Distributed Operation**Require:**

Switching point: U_{switch}
 SE threshold: η_{th}
 Subarray selection sets: $\{\mathcal{D}_i\}_{i \in \mathcal{K}}$
 Channel statistics: $\{\mathbf{Q}_{kl}, \mathbf{R}_{kl}\}_{k \in \mathcal{K}, l \in \mathcal{D}}, \{\beta_k\}_{k \in \mathcal{K}}$
 Transmit powers: $\{p_k\}_{k \in \mathcal{K}}$

Ensure:

Set of scheduled users: \mathcal{U}
 Pilot indices: $\{t_k\}_{k \in \mathcal{U}}$
 Weights: $\{\mu_{kl}\}_{k \in \mathcal{U}, l \in \mathcal{D}_k}$

1: Initialize: $\mathcal{U} \leftarrow \emptyset, \tau_p \leftarrow 0, \eta_{\min} \leftarrow 2\eta_{\text{th}}$
 2: **while** $|\mathcal{U}| < K$ and $\eta_{\min} > \eta_{\text{th}}$ **do**
 3: $k \leftarrow \arg \max_{i \in \mathcal{K} \setminus \mathcal{U}} \beta_i$ and $\tilde{\mathcal{U}} \leftarrow \mathcal{U} \cup \{k\}$
 4: **for** $t = 1$ to $\tau_p + 1$ **do**
 5: $t_k \leftarrow t, \tau \leftarrow \max(\tau_p, t_k), \zeta \leftarrow \{1, \dots, \tau\}$
 6: $\Psi_{\tilde{t}l} \leftarrow \sum_{i \in \tilde{\mathcal{U}}} p_i \tau \mathbf{R}_{il} + \sigma_n^2 \mathbf{I}_M, l \in \mathcal{D}, \tilde{t} \in \zeta$
 7: $\mathbf{C}_{il} \leftarrow \mathbf{R}_{il} - p_i \tau \mathbf{R}_{il} \Psi_{\tilde{t}l}^{-1} \mathbf{R}_{il}, l \in \mathcal{D}, i \in \tilde{\mathcal{U}}$
 8: $\mathbf{S}_{il} = \mathbf{Q}_{il} - \mathbf{C}_{il}, l \in \mathcal{D}, i \in \tilde{\mathcal{U}}$
 9: **if** $|\tilde{\mathcal{U}}| > U_{\text{switch}}$ **then**: for $i \in \tilde{\mathcal{U}}$ and $l \in \mathcal{D}_i$:
 10: $\bar{\mathbf{Z}}_{il} \leftarrow \sum_{i' \in \tilde{\mathcal{U}} \setminus \{i\}} p_{i'} \mathbf{Q}_{i'l} + p_i \mathbf{C}_{il} + \sigma_n^2 \mathbf{I}_M$
 11: $\Gamma_{il} \leftarrow p_i \text{tr}[\bar{\mathbf{Z}}_{il}^{-1} (\mathbf{Q}_{il} - \mathbf{C}_{il})]$
 12: **else**: for $i \in \tilde{\mathcal{U}}$ and $l \in \mathcal{D}_i$:
 13: $\Gamma_{il} \leftarrow \frac{\text{tr}(\mathbf{S}_{il}) - \sum_{i' \in \tilde{\mathcal{U}} \setminus \{i\}} \frac{\text{tr}(\mathbf{S}_{i'l})}{\text{tr}(\mathbf{S}_{i'l})}}{\sum_{i' \in \tilde{\mathcal{U}}} \frac{p_{i'}}{M p_i} \text{tr}(\mathbf{C}_{i'l}) + \sigma_n^2}$
 14: **end if**
 15: $\mu_{il}^{(t)} \leftarrow \Gamma_{il} / \sum_{l' \in \mathcal{D}_i} \Gamma_{il'}, i \in \tilde{\mathcal{U}} \text{ and } l \in \mathcal{D}_i$
 16: $\eta_{\min}^{(t)} \leftarrow \min_{i \in \tilde{\mathcal{U}}} \left(1 - \frac{\tau}{\tau_c} \right) \log_2 \left(1 + \sum_{l \in \mathcal{D}_i} \Gamma_{il} \right)$
 17: **end for**
 18: $t_k \leftarrow \arg \max_{t \in \{1, \dots, \tau_p + 1\}} \eta_{\min}^{(t)}$ and $\eta_{\min} \leftarrow \eta_{\min}^{(t_k)}$
 19: **if** $\eta_{\min} \geq \eta_{\text{th}}$ **then**
 20: $\mathcal{U} \leftarrow \tilde{\mathcal{U}}$ and $\tau_p \leftarrow \max(\tau_p, t_k)$
 21: $\mu_{il} \leftarrow \mu_{il}^{(t_k)}, i \in \mathcal{U} \text{ and } l \in \mathcal{D}_i$
 22: **end if**
 23: **end while**

mates the global SINR as the sum of the local SINRs at the selected subarrays, following Proposition 1.

A. Performance Evaluation

This subsection assesses the efficacy of the proposed algorithms in maximizing the minimum per-user SE, demonstrating that strategies based on deterministic SINR expressions achieve performance comparable to those based on instantaneous SINR, but with significantly reduced computational complexity. We assume $L = 16$, $L_k = 4$, and $M = 16$, with the simulation setup following the parameters established in Section III-A. Since LSF-based subarray selection yields performance comparable to the SINR-based strategy (as shown in Section III-A), it is adopted hereafter for its lower complexity.

Figure 5 depicts the minimum per-user SE as a function of the number of scheduled users (U). We compare Algorithms 2 and 3 (labeled *Max-Min SE (Ana)*) against a numerical benchmark, *Max-Min SE (Num)*. This benchmark follows the same logic as the proposed algorithms but utilizes the numerical mean SINR for pilot assignment instead of the derived deterministic approximations. Two baselines serve as references: Algorithm 1, which is labeled *Orthogonal* since it assigns mutually orthogonal pilots by minimizing the maximum channel estimation NMSE, and a *Random* pilot assignment. All schemes employ user scheduling based on descending LSF gains and LSF-based subarray selection. The scenario features $K = 16$ UEs and a short coherence block ($\tau_c = 10$), rendering pilot contamination unavoidable.⁷

Figures 5a and 5b, corresponding to centralized and distributed architectures respectively, show that the centralized approach consistently yields a higher minimum SE. This is expected, as the CPU in a centralized architecture jointly processes signals from all L_k selected subarrays, enabling global interference suppression. Conversely, the distributed architecture relies on local combining, limiting interference mitigation capabilities. Notably, if each UE were served by a single subarray ($L_k = 1$), both architectures would converge to identical performance.

In both architectures, the *Max-Min SE (Num)* strategy effectively mitigates interference by leveraging the true mean SINR; however, it incurs prohibitive computational costs by relying on extensive instantaneous CSI processing. In contrast, the *Max-Min SE (Ana)* strategy achieves remarkably similar performance using only deterministic SINR approximations, offering a tractable solution. The negligible performance gap suggests that the primary gains in pilot assignment stem from resolving large-scale spatial conflicts, which the derived deterministic expressions capture efficiently without requiring Monte Carlo sampling or instantaneous fading optimization.

⁷Results are plotted up to the full load $U = K$ for illustrative purposes. In practice, the algorithm terminates when the SE threshold is violated, potentially leaving some UEs unscheduled.

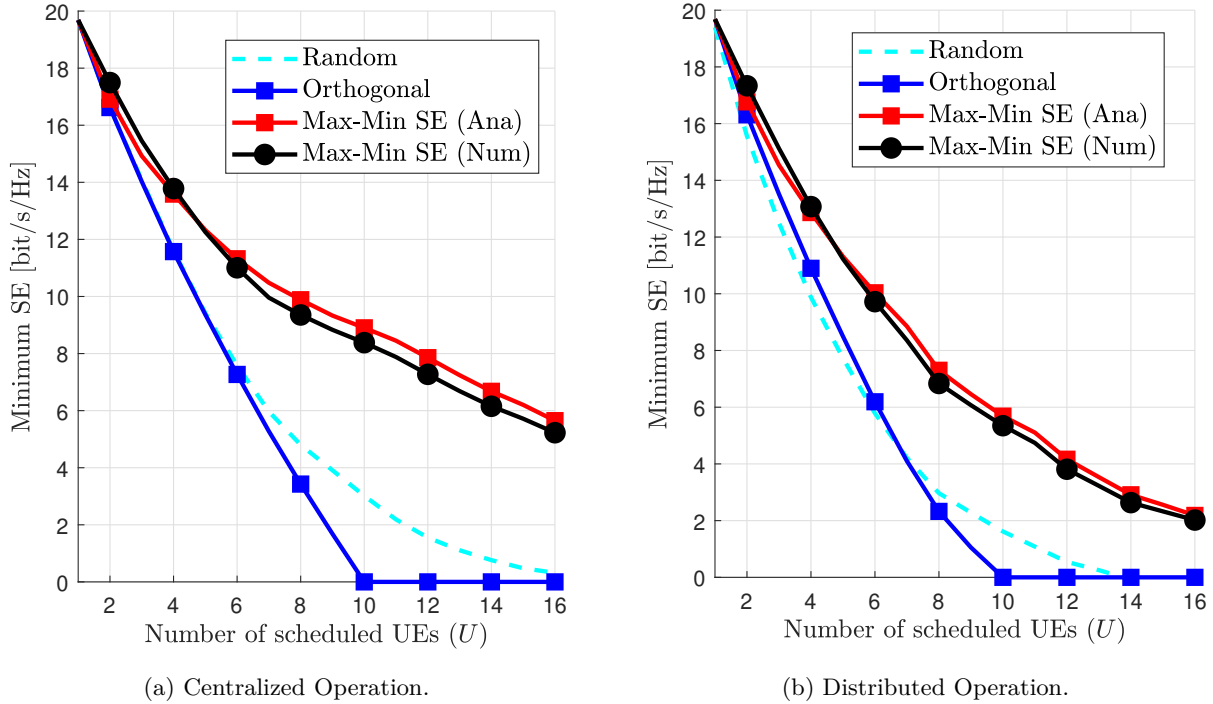


Figure 5. Minimum per-user SE versus number of scheduled UEs.

Furthermore, the proposed strategy rivals the numerical benchmark in maximizing the number of scheduled UEs that satisfy a per-user SE requirement. For instance, given a 5 bit/s/Hz threshold in Fig. 5a, the *Random* and *Orthogonal* baselines schedule only 7 UEs, whereas both *max-min* algorithms successfully schedule all 16 UEs. These results highlight the effectiveness of deterministic SINR-based resource allocation in enhancing fairness within crowded XL-MIMO networks.

While the intelligent strategies maintain robust performance as U increases, the *Random* and *Orthogonal* assignments suffer severe degradation due to uncoordinated pilot reuse and reduced data transmission intervals (caused by increasing pilot sequence lengths), respectively.

Finally, Figure 6 illustrates the minimum per-user SE as a function of the coherence block length (τ_c) for $K = 6$ UEs. A *Max-Min SE (Num - Exhaustive Search)* benchmark is introduced to establish the theoretical performance upper bound. Unlike the sequential approach of the *Max-Min SE (Num)* strategy—where pilots are assigned one-by-one to newly scheduled UEs without re-evaluating previous assignments—the exhaustive search evaluates all possible pilot combinations to identify the global optimum.

Notably, the sequential mechanism employed by the proposed Algorithms 2 and 3 proves highly effective, achieving performance nearly identical to the optimal exhaustive search. Moreover, results

suggest that the *Max-Min SE (Ana)* approach may approximate the optimal pilot assignment even more closely than the numerical version. This aligns with observations in Figure 5, where the analytical strategy occasionally outperforms the *Max-Min SE (Num)* benchmark, likely because the deterministic expressions effectively capture long-term spatial conflicts without the variance associated with limited instantaneous SINR samples.

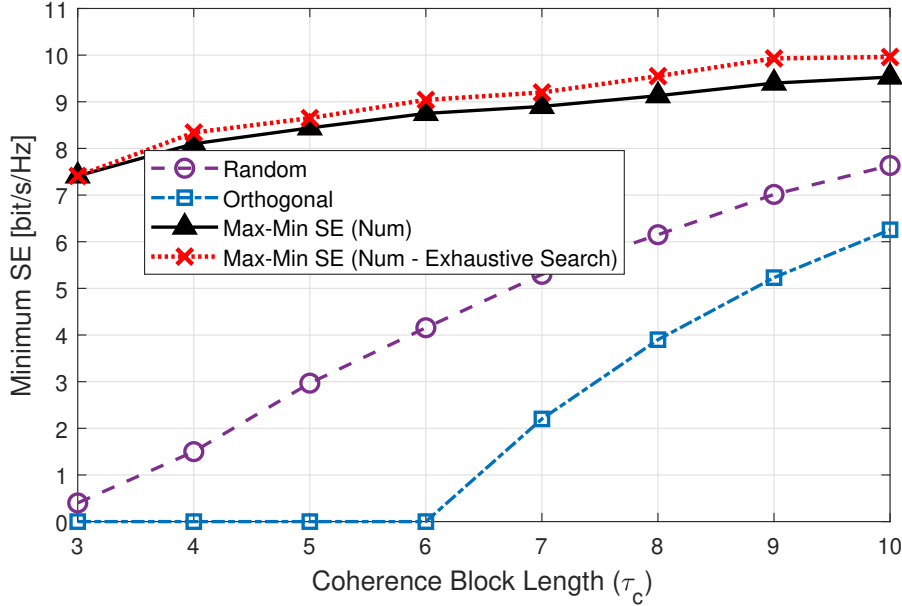


Figure 6. Minimum per-user SE versus coherence block length.

V. CONCLUSION

This paper addressed the critical challenge of resource allocation in XL-MIMO systems, where the reliance on instantaneous CSI for optimization is computationally prohibitive. We introduced novel, closed-form deterministic SINR expressions for both centralized and distributed uplink operations. These expressions, which are valid for Rician fading channels and account for MMSE receive combining and channel estimation, depend exclusively on long-term channel statistics. This key innovation provides a tractable analytical foundation for XL-MIMO system design and optimization, eliminating the need for computationally expensive instantaneous CSI.

Building on these theoretical results, we developed a suite of low-complexity algorithms for joint subarray selection, user scheduling, and pilot assignment. By leveraging the derived statistical SINR approximations, these algorithms are designed to maximize the minimum spectral efficiency among scheduled users, thereby enhancing fairness. Our numerical results validate the high accuracy of the

SINR approximations and demonstrate that the proposed statistical-CSI-driven framework achieves performance remarkably close to that of instantaneous-CSI-based benchmarks. The proposed methods effectively exploit the spatial sparsity of user visibility regions to enable more aggressive pilot reuse, significantly improving both fairness and throughput in crowded network scenarios. This work demonstrates that by relying on slowly-varying channel statistics, it is possible to design resource allocation schemes that are both highly efficient and practical for real-world XL-MIMO deployments.

A. Future Research Directions

The findings of this work open up several promising avenues for future research, including:

- *Hardware Impairments and Channel Aging:* Future studies could extend the deterministic SINR framework to incorporate the effects of practical hardware impairments, such as phase noise and power amplifier nonlinearity, as well as channel aging in high-mobility scenarios. Developing robust resource allocation algorithms would be a significant step toward practical implementation.
- *Downlink Transmission and Precoding Design:* This work focused exclusively on the uplink. A natural extension is to develop a similar statistical-CSI-based framework for the downlink, including the design of low-complexity precoding schemes that can achieve near-optimal performance without requiring instantaneous CSI at the transmitter.
- *Energy Efficiency Optimization:* While the proposed algorithms enhance spectral efficiency and fairness, they do not explicitly consider energy consumption. Future research could focus on developing resource allocation strategies that jointly optimize for spectral and energy efficiency, a critical requirement for sustainable 6G networks.
- *Machine Learning-based Approaches:* The statistical nature of the proposed framework makes it well-suited for machine learning-based enhancements. Deep learning models could be trained to learn the complex relationships between long-term channel statistics and optimal resource allocation decisions, potentially leading to even lower-complexity and more adaptive solutions.
- *Integration with Reconfigurable Intelligent Surfaces (RIS):* The synergy between XL-MIMO and RIS is a promising area of investigation. Future work could explore the joint design of subarray selection in XL-MIMO and passive beamforming at the RIS, leveraging statistical CSI to create a programmable and highly efficient wireless environment.
- *Near-Field Communications:* As XL-MIMO systems operate in the near-field, future research should more deeply investigate the implications of spherical wave propagation on channel modeling and resource allocation. Extending the deterministic SINR expressions to explicitly account for near-field effects would provide a more accurate analytical foundation for such systems.

APPENDIX A
PROOF OF PROPOSITION 1

When $M \geq U$, the local ZF combiner satisfies $\mathbf{v}_{kl}^H \hat{\mathbf{h}}_{il} = \delta_{ik}$. Under high signal-to-noise ratio (SNR) and small channel estimation errors, the L-MMSE combiner converges to the local ZF, and thus obeys the approximation $\mathbf{v}_{kl}^H \hat{\mathbf{h}}_{il} \approx \delta_{ik}$, yielding the local and global SINR approximations given by

$$\Gamma_{kl} \approx \frac{p_k}{\mathbf{v}_{kl}^H \left(\sum_{i \in \mathcal{U}} p_i \mathbf{C}_{il} + \sigma_n^2 \mathbf{I}_M \right) \mathbf{v}_{kl}}, \quad (39)$$

$$\Gamma_k \approx \frac{p_k}{\sum_{l \in \mathcal{D}_k} \mu_{kl}^2 \mathbf{v}_{kl}^H \left(\sum_{i \in \mathcal{U}} p_i \mathbf{C}_{il} + \sigma_n^2 \mathbf{I}_M \right) \mathbf{v}_{kl}}. \quad (40)$$

Corollary 1 follows directly by rewriting (40) and comparing it with the approximation of Γ_{kl}^{-1} in (39):

$$\Gamma_k^{-1} \approx \sum_{l \in \mathcal{D}_k} \mu_{kl}^2 \underbrace{\frac{1}{p_k} \mathbf{v}_{kl}^H \left(\sum_{i \in \mathcal{U}} p_i \mathbf{C}_{il} + \sigma_n^2 \mathbf{I}_M \right) \mathbf{v}_{kl}}_{\Gamma_{kl}^{-1}}.$$

Although L-MMSE and local ZF combiners perform similarly only under low channel estimation errors, the accuracy of the approximation (26) may improve as these errors grow. The resulting increase in \mathbf{C}_{il} dominates the SINR denominator, rendering the neglected interference terms $\mathbf{v}_{kl}^H \hat{\mathbf{h}}_{il}$ negligible compared to the $\mathbf{v}_{kl}^H \mathbf{C}_{il} \mathbf{v}_{kl}$ components.

The optimal weights for distributed uplink operation are obtained by maximizing the approximate global SINR in (24), given the local SINRs. As $\mu_{kl} \geq 0$ and $\Gamma_{kl} \geq 0$ for all $l \in \mathcal{D}_k$, we have $\sum_{l \in \mathcal{D}_k} \mu_{kl}^2 \Gamma_{kl}^{-1} > 0$. Thus, maximizing $\hat{\Gamma}_k$ is equivalent to solving

$$\min_{\{\mu_{kl}\}_{l \in \mathcal{D}_k}} \sum_{l \in \mathcal{D}_k} \mu_{kl}^2 \Gamma_{kl}^{-1} \quad (41a)$$

$$\text{s.t.} \quad \sum_{l \in \mathcal{D}_k} \mu_{kl} = 1, \quad (41b)$$

$$\mu_{kl} \geq 0, \quad \forall l \in \mathcal{D}_k, \quad (41c)$$

where constraints (41b) and (41c) enforce nonnegative, unit-sum weights. Neglecting (41c), which

will be satisfied a posteriori, the Lagrangian is

$$\mathcal{L}_k = \sum_{l \in \mathcal{D}_k} \mu_{kl}^2 \Gamma_{kl}^{-1} + \lambda_k \left(\sum_{l \in \mathcal{D}_k} \mu_{kl} - 1 \right), \quad (42)$$

where λ_k is the lagrangian multiplier. The first-order optimality condition gives [42]

$$\frac{\partial \mathcal{L}_k}{\partial \mu_{kl}} = 2\Gamma_{kl}^{-1} \mu_{kl} + \lambda_k = 0, \quad l \in \mathcal{D}_k, \quad (43)$$

which yields

$$\mu_{kl} = -\frac{1}{2} \Gamma_{kl} \lambda_k, \quad l \in \mathcal{D}_k. \quad (44)$$

Substituting (44) into (41b) results in $\lambda_k = -\frac{2}{\sum_{l \in \mathcal{D}_k} \Gamma_{kl}}$. Substituting this into (44) completes the proof of (25), and inserting (25) into (24) yields (26).

APPENDIX B

PROOF OF THEOREM 1

We first establish the following lemma regarding the expectation of the inverse of a random matrix.

Lemma 1. *Let \mathbf{X} be an invertible random matrix with mean $\mathbf{A} = \mathbb{E}\{\mathbf{X}\}$. If the fluctuation $\Delta = \mathbf{X} - \mathbf{A}$ is sufficiently small to satisfy $\|\mathbf{A}^{-1}\Delta\| < 1$, then the approximation $\mathbb{E}\{\mathbf{X}^{-1}\} \approx (\mathbb{E}\{\mathbf{X}\})^{-1}$ holds.*

Proof. Using the Neumann series expansion [43], we have $\mathbf{X}^{-1} = (\mathbf{A} + \Delta)^{-1} = \mathbf{A}^{-1} \sum_{n=0}^{\infty} (-1)^n (\Delta \mathbf{A}^{-1})^n$. For small Δ , truncating the series at $n = 0$ and taking the expectation (noting that $\mathbb{E}\{\Delta\} = \mathbf{0}$) yields $\mathbb{E}\{\mathbf{X}^{-1}\} = \mathbf{A}^{-1} + \mathcal{O}(\mathbb{E}\{\|\Delta\|^2\})$, which justifies the approximation. \square

The average local SINR in (20) can be expressed as

$$\mathbb{E}\{\Gamma_{kl}\} = p_k \operatorname{tr}(\mathbb{E}\{\mathbf{Z}_{kl}^{-1} \hat{\mathbf{h}}_{kl} \hat{\mathbf{h}}_{kl}^H\}). \quad (45)$$

Under typical pilot-reuse patterns (where few or no UEs share the pilot of UE k) and limited LoS overlap across subarrays, \mathbf{Z}_{kl} and $\hat{\mathbf{h}}_{kl}$ are approximately uncorrelated. Thus,

$$\mathbb{E}\{\mathbf{Z}_{kl}^{-1} \hat{\mathbf{h}}_{kl} \hat{\mathbf{h}}_{kl}^H\} \approx \mathbb{E}\{\mathbf{Z}_{kl}^{-1}\} (\mathbf{Q}_{kl} - \mathbf{C}_{kl}). \quad (46)$$

Furthermore, when $U \gg M$ or when subarray selection favors subarrays with a strong LoS component to UE k , the matrix \mathbf{Z}_{kl} concentrates around its mean $\bar{\mathbf{Z}}_{kl} = \mathbb{E}\{\mathbf{Z}_{kl}\}$. In this regime, \mathbf{Z}_{kl} exhibits small fluctuations, and Lemma 1 implies

$$\mathbb{E}\{\mathbf{Z}_{kl}^{-1}\} \approx (\mathbb{E}\{\mathbf{Z}_{kl}\})^{-1} = \bar{\mathbf{Z}}_{kl}^{-1}. \quad (47)$$

Substituting (47) into (46) yields

$$\mathbb{E}\{\mathbf{Z}_{kl}^{-1}\hat{\mathbf{h}}_{kl}\hat{\mathbf{h}}_{kl}^H\} \approx \bar{\mathbf{Z}}_{kl}^{-1}(\mathbf{Q}_{kl} - \mathbf{C}_{kl}). \quad (48)$$

Inserting (48) into (45) completes the proof of (30b). The proof of (30a) follows similar steps.

APPENDIX C

PROOF OF COROLLARY 1

Evaluating (30b) primarily involves computing the trace $\text{tr}(\mathbf{A}^{-1}\mathbf{B})$, where $\mathbf{A} = \bar{\mathbf{Z}}_{kl}$ and $\mathbf{B} = \mathbf{Q}_{kl} - \mathbf{C}_{kl}$. Let $\mathbf{C} = \mathbf{A}^{-1}\mathbf{B}$. We efficiently compute the diagonal elements of \mathbf{C} by solving the linear systems $\mathbf{A}\mathbf{c}_m = \mathbf{b}_m$ for $m = 1, \dots, M$, where \mathbf{c}_m and \mathbf{b}_m are the m -th columns of \mathbf{C} and \mathbf{B} , respectively.

First, the \mathbf{LDL}^H decomposition of the Hermitian matrix \mathbf{A} requires $\frac{1}{3}(M^3 - M)$ complex multiplications [41, App. B.1.1]. The system $\mathbf{LDL}^H\mathbf{c}_m = \mathbf{b}_m$ is then solved for the m -th row of each column \mathbf{c}_m in three steps: (i) solving $\mathbf{L}\mathbf{z}_m = \mathbf{b}_m$ for each m requires a total of $M \times \frac{1}{2}(M^2 - M)$ complex multiplications; (ii) solving $\mathbf{D}\mathbf{y}_m = \mathbf{z}_m$ involves M complex-by-real divisions per column, *i.e.*, $M \times 2M = 2M^2$ real divisions; and (iii) to obtain the diagonal element $[\mathbf{c}_m]_m$, the system $\mathbf{L}^H\mathbf{c}_m = \mathbf{y}_m$ is solved from the M -th row up to the m -th row, which requires $\sum_{n=0}^{M-m} n = \frac{(M-m)(M-m+1)}{2}$ complex multiplications. Hence, the total cost for all $m = 1, \dots, M$ is $\sum_{m=1}^M \frac{(M-m)(M-m+1)}{2} = \frac{M^3 - M}{6}$ complex multiplications.

Assuming each complex multiplication is implemented via three real multiplications and each real division is computationally equivalent to a real multiplication [41, App. B.1.1], the total complexity of computing Γ_{kl}^{erg} across the L_k subarrays that serve UE k is equivalent to $\mathcal{C}_k^{\text{erg}} = L_k[M^3 - M + \frac{3}{2}(M^3 - M^2) + 2M^2 + \frac{1}{2}(M^3 - M)]$ real multiplications, which simplifies to (32b). The proof of (32a) follows similar steps, by substituting the subarray antenna dimension M with the total number of serving antennas ML_k .

APPENDIX D
PROOF OF THEOREM 2

Under the assumption of spatially uncorrelated NLoS components, where $\mathbf{C}_{il} = \frac{1}{M} \text{tr}(\mathbf{C}_{il}) \mathbf{I}_M$, the instantaneous SINR approximation in (39) reduces to⁸

$$\Gamma_{kl} \approx \frac{p_k}{\left(\sum_{i \in \mathcal{U}} \frac{p_i}{M} \text{tr}(\mathbf{C}_{il}) + \sigma_n^2 \right) \|\mathbf{v}_{kl}\|^2}. \quad (49)$$

The term $\|\mathbf{v}_{kl}\|^2$ is approximated using the local-ZF combiner, which behaves similarly to the L-MMSE combiner at high SNR and sufficiently accurate channel estimates. Letting $\mathcal{U} = \mathcal{K}$, the local ZF matrix at subarray l is $\mathbf{V}_l = \widehat{\mathbf{H}}_l (\widehat{\mathbf{H}}_l^H \widehat{\mathbf{H}}_l)^{-1}$, where $\widehat{\mathbf{H}}_l = [\widehat{\mathbf{h}}_{1l}, \dots, \widehat{\mathbf{h}}_{Kl}]$ and \mathbf{v}_{kl} is the k -th column of \mathbf{V}_l . The block matrix inversion lemma yields [26, Appendix A]

$$\begin{aligned} \|\mathbf{v}_{kl}\|^2 &= [\mathbf{V}_l^H \mathbf{V}_l]_{k,k} = [(\widehat{\mathbf{H}}_l^H \widehat{\mathbf{H}}_l)^{-1}]_{k,k} \\ &= [\widehat{\mathbf{h}}_{kl}^H (\mathbf{I}_M - \mathbf{P}_{kl}) \widehat{\mathbf{h}}_{kl}]^{-1}, \end{aligned} \quad (50)$$

where $\mathbf{P}_{kl} = \ddot{\mathbf{H}}_{kl} (\ddot{\mathbf{H}}_{kl}^H \ddot{\mathbf{H}}_{kl})^{-1} \ddot{\mathbf{H}}_{kl}^H$ and $\ddot{\mathbf{H}}_{kl} \in \mathbb{C}^{M \times (K-1)}$ denotes the estimated channel matrix at subarray l excluding UE k . Substituting (50) into (49) results in

$$\Gamma_{kl} \approx p_k \frac{\widehat{\mathbf{h}}_{kl}^H (\mathbf{I}_M - \mathbf{P}_{kl}) \widehat{\mathbf{h}}_{kl}}{\sum_{i \in \mathcal{U}} \frac{p_i}{M} \text{tr}(\mathbf{C}_{il}) + \sigma_n^2}. \quad (51)$$

Lemma 2. *The cross-correlation between the MMSE estimates $\widehat{\mathbf{h}}_{kl}$ and $\widehat{\mathbf{h}}_{il}$ is given by [5, page 107]:*

$$\mathbb{E}\{\widehat{\mathbf{h}}_{kl} \widehat{\mathbf{h}}_{il}^H\} = \begin{cases} \mathbf{Q}_{kl} - \mathbf{C}_{kl}, & i = k, \\ \overline{\mathbf{h}}_{kl} \overline{\mathbf{h}}_{il}^H + \mathbf{A}_{kil}, & t_i = t_k, \\ \overline{\mathbf{h}}_{kl} \overline{\mathbf{h}}_{il}^H, & \text{otherwise,} \end{cases} \quad (52)$$

where $\mathbf{A}_{kil} = \sqrt{p_k p_i} \tau_p \mathbf{R}_{kl} \Psi_{tkl}^{-1} \mathbf{R}_{il}$. Furthermore, for any matrices $\mathbf{A}, \mathbf{B} \in \mathbb{C}^{M \times M}$ independent of the channel estimates, the quadratic form $\widehat{\mathbf{h}}_{il}^H \mathbf{B} \mathbf{A} \widehat{\mathbf{h}}_{kl}$ converges to its expectation as $M \rightarrow \infty$ [33, Lemma 4]:

$$\widehat{\mathbf{h}}_{il}^H \mathbf{B} \mathbf{A} \widehat{\mathbf{h}}_{kl} \xrightarrow[M \rightarrow \infty]{a.s.} \mathbb{E}\{\widehat{\mathbf{h}}_{il}^H \mathbf{B} \mathbf{A} \widehat{\mathbf{h}}_{kl}\} = \text{tr}(\mathbf{A} \mathbb{E}\{\widehat{\mathbf{h}}_{kl} \widehat{\mathbf{h}}_{il}^H\} \mathbf{B}). \quad (53)$$

⁸This remains accurate for correlated NLoS components in the absence of pilot reuse. This is because the eigenvalues of the matrix term within parentheses in (39) are closely clustered without pilot reuse. Thus, the SINR denominator presents negligible variations when replacing \mathbf{C}_{il} with $\frac{1}{M} \text{tr}(\mathbf{C}_{il}) \mathbf{I}_M$.

Applying (52), this yields

$$\hat{\mathbf{h}}_{il}^H \mathbf{B} \mathbf{A} \hat{\mathbf{h}}_{kl} \xrightarrow[M \rightarrow \infty]{a.s.} \begin{cases} \text{tr}[\mathbf{A}(\mathbf{Q}_{kl} - \mathbf{C}_{kl})\mathbf{B}], & i = k, \\ \text{tr}[\mathbf{A}(\bar{\mathbf{h}}_{kl} \bar{\mathbf{h}}_{il}^H + \mathbf{A}_{kil})\mathbf{B}], & t_i = t_k, \\ \bar{\mathbf{h}}_{il}^H \mathbf{B} \mathbf{A} \bar{\mathbf{h}}_{kl}, & t_i \neq t_k. \end{cases} \quad (54)$$

The diagonal elements of $\ddot{\mathbf{H}}_{kl}^H \ddot{\mathbf{H}}_{kl}$ consist of the squared norms $\|\hat{\mathbf{h}}_{il}\|^2$ for $i \in \mathcal{K} \setminus \{k\}$, which converge to $\text{tr}(\mathbf{Q}_{il} - \mathbf{C}_{il})$ as $M \rightarrow \infty$, according to (54). In XL-MIMO, the off-diagonal terms are negligible due to the channel spatial non-stationarity.⁹ We can thus approximate (51) by

$$\Gamma_{kl} \approx p_k \frac{\hat{\mathbf{h}}_{kl}^H \hat{\mathbf{h}}_{kl} - \hat{\mathbf{h}}_{kl}^H \ddot{\mathbf{H}}_{kl} \mathbf{T}_{kl}^{-1} \ddot{\mathbf{H}}_{kl}^H \hat{\mathbf{h}}_{kl}}{\sum_{i \in \mathcal{U}} \frac{p_i}{M} \text{tr}(\mathbf{C}_{il}) + \sigma_n^2}. \quad (55)$$

where $\mathbf{T}_{kl} = \text{diag}(\{\|\hat{\mathbf{h}}_{il}\|^2\}_{i \in \mathcal{U} \setminus \{k\}})$ contains only the diagonal terms of $\ddot{\mathbf{H}}_{kl}^H \ddot{\mathbf{H}}_{kl}$.

Applying the asymptotic results from (54), the terms in the numerator converge as follows:

$$\hat{\mathbf{h}}_{kl}^H \hat{\mathbf{h}}_{kl} \xrightarrow{M \rightarrow \infty} \text{tr}(\mathbf{Q}_{kl} - \mathbf{C}_{kl}) \quad (56)$$

and

$$\begin{aligned} \hat{\mathbf{h}}_{kl}^H \ddot{\mathbf{H}}_{kl} \mathbf{T}_{kl}^{-1} \ddot{\mathbf{H}}_{kl}^H \hat{\mathbf{h}}_{kl} &= \sum_{i \in \mathcal{U} \setminus \{k\}} \frac{\hat{\mathbf{h}}_{kl}^H \hat{\mathbf{h}}_{il} \hat{\mathbf{h}}_{il}^H \hat{\mathbf{h}}_{kl}}{\hat{\mathbf{h}}_{il}^H \hat{\mathbf{h}}_{il}} \\ &\xrightarrow{M \rightarrow \infty} \frac{\text{tr}(\mathbf{X}_{kl} \mathbf{X}_{il})}{\text{tr}(\mathbf{X}_{il})}. \end{aligned} \quad (57)$$

Substituting these into (55) concludes the proof of (33b). The proof of (33a) follows similar steps.

REFERENCES

- [1] Z. Wang, J. Zhang, H. Du, D. Niyato, S. Cui, B. Ai, M. Debbah, K. B. Letaief, and H. V. Poor, “A tutorial on extremely large-scale MIMO for 6G: Fundamentals, signal processing, and applications,” *IEEE Communications Surveys & Tutorials*, vol. 26, no. 3, pp. 1560–1605, 2024.
- [2] J. G. Andrews, S. Buzzi, W. Choi, S. V. Hanly, A. Lozano, A. C. K. Soong, and J. C. Zhang, “What will 5G be?” *IEEE Journal on Selected Areas in Communications*, vol. 32, no. 6, pp. 1065–1082, 2014.
- [3] M. Shafi, A. F. Molisch, P. J. Smith, T. Haustein, P. Zhu, P. De Silva, F. Tufvesson, A. Benjebbour, and G. Wunder, “5G: A tutorial overview of standards, trials, challenges, deployment, and practice,” *IEEE Journal on Selected Areas in Communications*, vol. 35, no. 6, pp. 1201–1221, 2017.

⁹From (54), the off-diagonal elements $\hat{\mathbf{h}}_{il}^H \hat{\mathbf{h}}_{i'l}$ ($i \neq i'$) converge to $\bar{\mathbf{h}}_{il}^H \bar{\mathbf{h}}_{i'l}$ as $M \rightarrow \infty$, since UEs are typically assigned distinct pilot sequences. In XL-MIMO, however, these off-diagonal terms are negligible compared to the diagonal components, since the large array dimensions ensure that LoS footprints of different UEs have minimal overlap across subarrays. This contrasts with conventional massive MIMO, where VRs typically encompass the entire co-located array.

- [4] M. Agiwal, A. Roy, and N. Saxena, "Next generation 5G wireless networks: A comprehensive survey," *IEEE Communications Surveys & Tutorials*, vol. 18, no. 3, pp. 1617–1655, 2016.
- [5] Özlem Tugfe Demir, E. Björnson, and L. Sanguinetti, "Foundations of user-centric cell-free massive MIMO," *Foundations and Trends® in Signal Processing*, vol. 14, no. 3-4, pp. 162–472, 2021. [Online]. Available: <http://dx.doi.org/10.1561/2000000109>
- [6] E. Björnson, L. Sanguinetti, H. Wymeersch, J. Hoydis, and T. L. Marzetta, "Massive MIMO is a reality—what is next?: Five promising research directions for antenna arrays," *Digital Signal Processing*, vol. 94, pp. 3–20, 2019.
- [7] Y. Han, S. Jin, C.-K. Wen, and X. Ma, "Channel estimation for extremely large-scale massive MIMO systems," *IEEE Wireless Communications Letters*, vol. 9, no. 5, pp. 633–637, 2020.
- [8] J. Zhang, J. Zhang, E. Björnson, and B. Ai, "Local partial zero-forcing combining for cell-free massive MIMO systems," *IEEE Transactions on Communications*, vol. 69, no. 12, pp. 8459–8473, 2021.
- [9] M. Cui, Z. Wu, Y. Lu, X. Wei, and L. Dai, "Near-field MIMO communications for 6G: Fundamentals, challenges, potentials, and future directions," *IEEE Communications Magazine*, vol. 61, no. 1, pp. 40–46, 2023.
- [10] E. D. Carvalho, A. Ali, A. Amiri, M. Angelichinoski, and R. W. Heath, "Non-stationarities in extra-large-scale massive MIMO," *IEEE Wireless Communications*, vol. 27, no. 4, pp. 74–80, 2020.
- [11] J. C. Marinello, T. Abrão, A. Amiri, E. de Carvalho, and P. Popovski, "Antenna selection for improving energy efficiency in XL-MIMO systems," *IEEE Transactions on Vehicular Technology*, vol. 69, no. 11, pp. 13 305–13 318, 2020.
- [12] D. Liu, J. Wang, Y. Li, Y. Han, R. Ding, J. Zhang, S. Jin, and T. Q. S. Quek, "Location-based visible region recognition in extra-large massive MIMO systems," *IEEE Transactions on Vehicular Technology*, vol. 72, no. 6, pp. 8186–8191, 2023.
- [13] J. H. I. de Souza, J. C. Marinello, A. Amiri, and T. Abrão, "Qos-aware user scheduling in crowded XL-MIMO systems under non-stationary multi-state LoS/NLoS channels," *IEEE Transactions on Vehicular Technology*, pp. 1–13, 2023.
- [14] S. Mashdour, A. R. Flores, S. Salehi, R. C. De Lamare, A. Schmeink, and P. B. Da Silva, "Robust resource allocation in cell-free massive MIMO systems," *IEEE Transactions on Communications*, pp. 1–1, 2025.
- [15] E. Björnson and L. Sanguinetti, "Making cell-free massive MIMO competitive with MMSE processing and centralized implementation," *IEEE Transactions on Wireless Communications*, vol. 19, no. 1, pp. 77–90, 2020.
- [16] S. Buzzi, C. D'Andrea, M. Fresia, Y.-P. Zhang, and S. Feng, "Pilot assignment in cell-free massive MIMO based on the hungarian algorithm," *IEEE Wireless Communications Letters*, vol. 10, no. 1, pp. 34–37, 2021.
- [17] K. Zhi, C. Pan, H. Ren, and K. Wang, "Ergodic rate analysis of reconfigurable intelligent surface-aided massive MIMO systems with ZF detectors," *IEEE Communications Letters*, vol. 26, no. 2, pp. 264–268, 2022.
- [18] C. D'Andrea, A. Garcia-Rodriguez, G. Geraci, L. G. Giordano, and S. Buzzi, "Analysis of UAV communications in cell-free massive MIMO systems," *IEEE Open Journal of the Communications Society*, vol. 1, pp. 133–147, 2020.
- [19] H. Lei, J. Zhang, Z. Wang, H. Xiao, and B. Ai, "Uplink performance of cell-free extremely large-scale MIMO systems," *IEEE Transactions on Vehicular Technology*, vol. 74, no. 5, pp. 8339–8344, 2025.
- [20] Y. Zhang, W. Xia, H. Zhao, Y. Mao, J. Zhang, and G. Zheng, "Enhancing uplink performance for cell-free massive MIMO with low-resolution ADCs by RSMA," *IEEE Journal on Selected Areas in Communications*, vol. 43, no. 3, pp. 720–735, 2025.

- [21] M. A. Hosany, "On the performance analysis of multi-user massive MIMO systems with error vector signals for 5G cellular networks," *Wireless Personal Communications*, vol. 123, no. 2, pp. 917–934, 2022. [Online]. Available: <https://doi.org/10.1007/s11277-021-09162-z>
- [22] J. Li, Q. Pan, Z. Wan, P. Zhu, D. Wang, M. Lou, J. Jin, F. Liu, and X. You, "Low altitude 3-D coverage performance analysis of cell-free RAN for 6G systems," *IEEE Transactions on Vehicular Technology*, vol. 72, no. 12, pp. 16 163–16 176, 2023.
- [23] S.-N. Jin, D.-W. Yue, and H. H. Nguyen, "Spectral and energy efficiency in cell-free massive MIMO systems over correlated rician fading," *IEEE Systems Journal*, vol. 15, no. 2, pp. 2822–2833, 2021.
- [24] Y. Fan, S. Wu, X. Bi, and G. Li, "Power allocation for cell-free massive MIMO ISAC systems with offs signal," *IEEE Internet of Things Journal*, vol. 12, no. 7, pp. 9314–9331, 2025.
- [25] X. Yang, F. Cao, M. Matthaiou, and S. Jin, "On the uplink transmission of extra-large scale massive MIMO systems," *IEEE Transactions on Vehicular Technology*, vol. 69, no. 12, pp. 15 229–15 243, 2020.
- [26] A. Ali, E. D. Carvalho, and R. W. Heath, "Linear receivers in non-stationary massive MIMO channels with visibility regions," *IEEE Wireless Communications Letters*, vol. 8, no. 3, pp. 885–888, June 2019.
- [27] S. Chen, J. Zhang, E. Björnson, J. Zhang, and B. Ai, "Structured massive access for scalable cell-free massive MIMO systems," *IEEE Journal on Selected Areas in Communications*, vol. 39, no. 4, pp. 1086–1100, 2021.
- [28] J. Qiu, K. Xu, X. Xia, Z. Shen, and W. Xie, "Downlink power optimization for cell-free massive MIMO over spatially correlated rayleigh fading channels," *IEEE Access*, vol. 8, pp. 56 214–56 227, 2020.
- [29] T. H. Nguyen, T. V. Chien, H. Q. Ngo, X. N. Tran, and E. Björnson, "Pilot assignment for joint uplink-downlink spectral efficiency enhancement in massive MIMO systems with spatial correlation," *IEEE Transactions on Vehicular Technology*, vol. 70, no. 8, pp. 8292–8297, 2021.
- [30] M. Zhou, Y. Zhang, X. Qiao, and L. Yang, "Spatially correlated rayleigh fading for cell-free massive MIMO systems," *IEEE Access*, vol. 8, pp. 42 154–42 168, 2020.
- [31] Q. Sun, X. Ji, Z. Wang, X. Chen, Y. Yang, J. Zhang, and K.-K. Wong, "Uplink performance of hardware-impaired cell-free massive MIMO with multi-antenna users and superimposed pilots," *IEEE Transactions on Communications*, vol. 71, no. 11, pp. 6711–6726, 2023.
- [32] N. Li and P. Fan, "Joint data power control and LSFD design in distributed cell-free massive MIMO under non-ideal ue hardware," *EURASIP Journal on Wireless Communications and Networking*, vol. 2024, no. 9, pp. 1–17, 2024. [Online]. Available: <https://doi.org/10.1186/s13638-024-02334-y>
- [33] S. Wagner, R. Couillet, M. Debbah, and D. T. M. Slock, "Large system analysis of linear precoding in correlated miso broADCast channels under limited feedback," *IEEE Transactions on Information Theory*, vol. 58, no. 7, pp. 4509–4537, 2012.
- [34] H. Haritha, D. N. Amudala, R. Budhiraja, and A. K. Chaturvedi, "Superimposed versus regular pilots for hardware impaired rician-faded cell-free massive MIMO systems," *IEEE Transactions on Communications*, vol. 72, no. 11, pp. 6688–6706, 2024.
- [35] V. Tentu, E. Sharma, D. N. Amudala, and R. Budhiraja, "UAV-enabled hardware-impaired spatially correlated cell-free massive MIMO systems: Analysis and energy efficiency optimization," *IEEE Transactions on Communications*, vol. 70, no. 4, pp. 2722–2741, 2022.
- [36] Z. Wang, J. Zhang, E. Björnson, and B. Ai, "Uplink performance of cell-free massive MIMO over spatially correlated rician fading channels," *IEEE Communications Letters*, vol. 25, no. 4, pp. 1348–1352, 2021.
- [37] X. Ma, X. Lei, P. T. Mathiopoulos, K. Yu, and X. Tang, "Scalable cell-free massive MIMO systems with

finite resolution ADCs/DACs over spatially correlated rician fading channels,” *IEEE Transactions on Vehicular Technology*, vol. 72, no. 6, pp. 7699–7716, 2023.

[38] H. Kaur and A. Kansal, “Closed-form analysis of RZF in multicell massive MIMO over correlated rician channel,” *Wireless Personal Communications*, vol. 131, no. 3, pp. 1685–1719, 2023. [Online]. Available: <https://doi.org/10.1007/s11277-023-10518-w>

[39] S. Mukherjee and R. Chopra, “Performance analysis of cell-free massive MIMO systems in LoS/ NLoS channels,” *IEEE Transactions on Vehicular Technology*, vol. 71, no. 6, pp. 6410–6423, 2022.

[40] O. Ozdogan, E. Bjornson, and E. G. Larsson, “Massive MIMO with spatially correlated rician fading channels,” *IEEE Transactions on Communications*, vol. 67, no. 5, pp. 3234–3250, 2019.

[41] E. Björnson, J. Hoydis, and L. Sanguinetti, “Massive MIMO networks: Spectral, energy, and hardware efficiency,” *Foundations and Trends® in Signal Processing*, vol. 11, no. 3-4, pp. 154–655, 2017. [Online]. Available: <http://dx.doi.org/10.1561/2000000093>

[42] S. Boyd and L. Vandenberghe, *Convex Optimization*. Cambridge University Press, 2004.

[43] R. A. Horn and C. R. Johnson, *Matrix Analysis*, 2nd ed. Cambridge University Press, 2012.